Comparative Study of Vibrational Raman Optical Activity with Different Time-Dependent Density Functional Approximations: The VROA36 Database

Pierpaolo Morgante, Herbert D. Ludowieg and Jochen Autschbach*

Department of Chemistry University at Buffalo State University of New York Buffalo, NY 14260-3000, USA email: jochena@buffalo.edu

August 2, 2022

Abstract

A new database, VROA36, is introduced to investigate the performance of computational approaches for vibrational Raman optical activity (VROA) calculations. The database is composed of 36 molecules with known experimental VROA spectra. It includes 93 conformers. Normal modes calculated with B3LYP-D3(BJ)/def2-TZVP are used to compute the VROA spectra with four functionals, B3LYP-D3(BJ), ω B97X-D, M11, and optimally tuned LC-PBE, and several basis sets. SimROA indices and frequency scaling factors are used to compare calculated spectra with each other and with experimental data. The four functionals perform equally well independently of the basis set, and achieve good agreement with the experimental data. For molecules near- or underresonance conditions, the inclusion of a complex (damped) linear response approach is important to obtain physically meaningful VROA intensities. We encourage the usage of any of the tested functional approximations for theoretical VROA studies and recommend the def2-SVPD Gaussian-type basis set for efficient and reliable calculations.

1 Introduction

The interaction between a chiral molecule and polarized electromagnetic radiation is the basis of many spectroscopic methods used in the chemical and biological sciences. ¹⁻⁶ One of the ultimate goals of *chiroptical* methods such as optical rotation (OR), electronic or vibrational circular dichroism (ECD, VCD), or circularly polarized luminescence (CPL) is to determine

the absolute configuration (AC) of a chiral molecule. Underlying these techniques is the differential complex refractive index of left and right circularly polarized light. Their routine application allows the investigation of molecules ranging from a few atoms up to the size of proteins, as well as other materials.^{7,8}

In more recent years, vibrational Raman optical activity (VROA) has emerged as new and powerful tool for the investigation of chiral molecules. 9,10 Its foundations were established in the early 1970s, 11-13 but the technique gained popularity only during the past two decades, mainly because of better instrumentation as well as the availability of commercial spectrometers. VROA measures the difference in the Raman scattering intensity of left and right circularly polarized light, and it can be applied to small and large molecules, proteins and even viruses.¹⁴ However—similar to other chiroptical methods—an experimental VROA spectrum alone is not sufficient to establish the AC of a chiral molecule, because there is no known simple relationship between the absolute signs of the spectral bands and the AC. The situation gets more complicated if the molecule has multiple chiral centers or groups, because then there may be multiple stereoisomers that need to be considered. It is precisely this scenario where vibrational optical activity shows considerable strength compared to OR and ECD or CPL, because different vibrational modes may be more sensitive to the chirality in different regions of the molecule. In the absence of structural data, for example from X-ray diffraction, the signs of the VROA bands for the different stereoisomers are most conveniently determined by quantum chemical calculations. 15-17 Of course, calculations are also vital for dissecting the physical origin of a particular VROA signal.¹⁸ This theoretical assistance for VROA specifically is in addition to the well-established fact that "it is virtually impossible to interpret and correctly assign the vibrational spectra of larger polyatomic molecules without quantum chemical calculations" (P. Pulay, in Reference 19).

The first calculation of a theoretical VROA spectrum was reported in 1989 for R-methylthiirane.²⁰ Since then, quantum chemistry methods to perform such calculations have been implemented in a variety of electronic structure theory programs. Due to a favorable performance-to-cost ratio, time-dependent density functional theory (TD-DFT) is the most popular framework for chiroptical calculations, including VROA.^{10,16,17,21} The Kohn-Sham (KS) formulation²² of DFT relies, of course, on approximations to the exchange-correlation functional. To date, there are hundreds of approximate functionals in the literature,²³ the accuracy of which is primarily determined by the 'ingredients' used in their definition (the electron density, reduced density gradients, the kinetic energy density, exact exchange, and so on).²⁴ Each functional has to be extensively tested to identify its strengths and weaknesses, as well as the reliability of its performance.

Systematic testing of exchange-correlation functionals is very common for ground-state

properties, and reference data for the evaluation of old and new approximations is collected in databases of chemical data such as GMTKN55, 25 MGCDB84, 26 and the Minnesota databases.²⁷ This approach was extended to excited state properties as well, with most of the effort in this direction having focused on excitation energies. ^{28–36} It appears that other properties have not yet received the same attention, although databases collecting optical rotation data are becoming more popular.³⁷⁻⁴⁰ Among them, the OR45 database developed by our group⁴¹ is one of the first examples. It includes 45 different molecules whose experimental molar optical rotations and ACs are known, and it was used to test five functionals (PBE0, 42,43 BHLYP,44,45 B3LYP,45-47 CAM-B3LYP,48 LC-PBE049) with a selection of eight different basis sets. The results obtained against the OR45 database showed that the calculated molar optical rotations are heavily influenced by the choice of the basis set. ORs are also strongly functional-dependent, as far as functional with different 'ingredients' (e.g., global hybrids vs. non-hybrids) are concerned. The variability among functionals belonging to the same class was found to be rather weak in comparison. A key step in a VROA calculation involves taking derivatives of the OR tensor elements with respect to the normal modes. It is therefore not too surprising that calculations have indicated that OR and VROA calculations share similar basis set dependencies. 41, 50, 51

Reiher and co-workers⁵⁰ investigated the performance of three functionals (SVWN, 52,53) BLYP, 45,46 and B3LYP) and six basis sets for the VROA of five small molecules. A few years later, Cheeseman and Frisch⁵¹ assembled a database of 11 molecules to test the basis set dependence of the VROA spectra computed with the B3LYP functional. They surveyed 16 basis sets, making the study the largest basis set assessment for VROA published so far. Both studies confirmed that the calculation of VROA spectra requires high-quality basis sets. Diffuse and polarization functions, even on hydrogen atoms (as first suggested previously by Zuber and Hug),⁵⁴ are important, originating in the relationship of VROA to the polarizability and OR tensors. The aug-cc-pVDZ basis⁵⁵ has become the *de facto* standard^{41,56-59} for optical activity (OA) calculations. The augmentation, however, renders this basis set somewhat problematic in applications to large molecules. Property-optimized basis sets aimed at reducing the cost of the calculations while keeping aug-cc-pVDZ accuracy were proposed for OA and VROA calculations. 54,59-63 These non-standard basis sets offer satisfactory performance for organic molecules, but they have so far not been defined and tested for organometallic systems and metal complexes. A basis set smaller than aug-cc-pVDZ that is available for most atom types and performs comparably well would therefore be desirable for OA calculations.

In this work, we aim at systematizing the computational study of VROA spectra. We introduce VROA36, a database of 36 molecules that includes 31 organic molecules and five transition metal complexes. Experimental spectra for these compounds, available in the lit-

erature, were recorded in condensed phase using three different incident wavelengths (488.0, 514.5, and 532.0 nm), which are in most cases far from resonance, but for some systems near electronic resonances. Three popular functionals for ground- and excited-state applications were tested, as well as an 'optimally tuned' range-separated hybrid (OT-RSH) functional whose range-separation parameter is optimized non-empirically for each molecule (details are given in Section 2). For systems where the incident laser photon energy is close to an electronic resonance, a 'damped' complex linear response TD-DFT method was used to obtain physically meaningful response functions. One major aim of the study was to test if different hybrid functionals produce large variations in the relative VROA intensities and signs of different vibrational modes. It was found that this is not the case. At the hybrid DFT/TD-DFT level, comparable VROA spectra are obtained with different functionals, across the set of molecules. Another aim was to test the performance of the augmented double- ζ def2-SVPD basis set⁶⁴ in VROA calculations across a set of diverse systems, to establish if it retains the favorable performance-to-cost ratio that is already documented for ground-state properties. Our results are in the affirmative.

2 Theoretical and Computational Details

All calculations were performed with KS DFT and KS TD-DFT linear response methods. Most calculations were performed with the Gaussian 16, version A.03 (G16) program.⁶⁹ The hybrid functional B3LYP-D3(BJ)^{45-47,70} and the def2-TZVP basis set⁶⁴ were employed for geometry optimizations and frequency calculations. We chose this functional because of its known excellent performance for geometry optimizations of small and large molecules,⁷¹⁻⁷⁴ as well as vibrational frequency calculations.⁷⁵⁻⁷⁸ The def2-TZVP basis set has been recommended as a good compromise between accuracy and cost,⁷⁷ and it is defined for all elements (H, C, N, O, F, S, Cl, Fe, Ni, Cu, Br, Zr, Rh) appearing in VROA36. The scalar relativistic effective core potential (ECP) paired with the def2-TZVP basis was used for zirconium and rhodium.

Modeling solvation effects—either implicitly or explicitly—would introduce a possible source of error cancellation, and possibly favor a functional/basis set combination rather than another. In addition, the wide range of solvents used in the experimental setups would restrain the functional assessment, as comparisons among different solvents would be required. To allow a broader performance evaluation, solvent effects were not generally considered in the computations. However, some test calculations were carried out to gauge the performance of a continuum solvation model, employing B3LYP-D3(BJ) with the aug-cc-pVDZ and def2-SVPD basis sets for d-glucose (8) and camphor (17). The conductor-like polarizable con-

tinuum model (C-PCM)^{79,80} was applied to re-optimize the molecular geometries and to add solvation effects on the calculation of the ROA intensities. The solvents used are water and tetrachloromethane, respectively (see **Section 4.4**). For flexible molecules, the CREST program^{81,82} was used to sample the conformer space and generate an initial set of structures. Final optimized structures within 2.5 kcal mol⁻¹ of the most stable conformer, as recommended by Nafie,¹⁰ were retained for the VROA analysis and included in the database.

For VROA intensity calculations, the B3LYP-D3(BJ), M11,⁸³ and ω B97X-D⁸⁴ functionals were employed with the aug-cc-pVDZ^{55,85-87} and def2-SVPD⁶⁴ basis sets and matching ECPs for heavy metals. The optimally-tuned LC-PBE functional^{88,89}(abbreviated here as γ^* -LC-PBE) was used with aug-cc-pVDZ only. Calculations of the Raman intensities for the two conformers of the iron complex **32** were affected by convergence issues that could not be resolved despite multiple attempts with different convergence algorithms. The cc-pVDZ and def2-SVP basis sets, i.e., without augmentation, were employed instead for these molecules only. As a side note, **32** belongs to a class of metal-helicene complexes for which a large body of work is available, showing that non-augmented basis sets are suitable for the description of their OR and other chiroptical properties by TD-DFT calculations.^{90,91} For a subset of molecules, calculations were also carried out with the def2-TZVPD⁶⁴ basis and the B3LYP-D3(BJ) functional.

For molecules having more than one conformer, the spectra presented in **Figures 5–7** and in the Supporting Information were obtained via Boltzmann averaging the individual spectra at 298.15 K. For each conformer, the Boltzmann weight was determined based on the calculated relative Gibbs free energy with respect to the lowest-energy conformer of each molecule. The Boltzmann-averaged spectra strongly reflect the appearance of the spectrum of the most abundant conformer, as one would expect. Inclusion of solvent effects and any changes in functional and basis set used for the geometry optimizations would slightly alter the geometries as well as the relative energies of the conformers, with repercussions on the shape of the calculated VROA spectra as well. To avoid an excessively large benchmark data set, the Boltzmann weights were therefore taken to correspond to the gas phase calculations with B3LYP-D3(BJ)/def2-TZVP, and they were applied to all functional/basis set combinations. The absolute and relative Gibbs free energies for each structure and the corresponding Boltzmann weights are reported in **Section S2** of the Supporting Information.

Most VROA spectra were calculated with the fully analytic gauge-independent atomic orbital (GIAO, 'London orbital')^{92,93} implementation in G16.⁹⁴ A developer's version for near- and on-resonance applications was reported,⁹⁵ but the available G16 implementation is presently limited to off-resonance cases. For VROA calculations of systems that are close to resonance with the incident laser, the complex response module of the NWChem pro-

gram^{96–98} was employed. Details about VROA calculations with this response code can be found in References 99 and 100. The relevant systems are 2-bromohexahelicene (24), naproxen (31), and the first-row transition-metal complexes (32–34 in Table 1). The value of the damping parameter Γ used to broaden the excited states was set to 0.0037 au, corresponding to a full width at half-maximum (FWHM) of 1600 cm⁻¹, consistent with previous work. 95,99,101-103 The NWChem program offers the possibility to run magnetic response calculations with and without GIAOs. We ran a set of B3LYP/aug-cc-pVDZ test calculations, which confirmed that NWChem calculations with GIAOs and without damping yield the same VROA intensities as the G16 code. Furthermore, there were negligible differences between test VROA spectra calculated with and without GIAOs, using a gauge origin at the center of nuclear charge of each molecule. Therefore, the rather demanding calculations for the near-resonance cases were performed without GIAOs, to reduce the need for computational resources. Caricato and Balduf recently introduced a way to calculate origin-invariant optical rotation without the need for GIAOs or the velocity gauge. 104 This approach seems promising for VROA calculations as well, but given the satisfactory performance of the present benchmark calculations, further testing of this approach in the VROA context will be left to a future study. All calculations used the experimental incident wavelengths listed in **Table 1** shown later.

Range-separation in DFT is built upon the idea of splitting the Coulomb operator into a short-range and long-range part. ¹⁰⁵ In the long-range correction (LC) scheme of Hirao and co-workers, ⁸⁹ the inverse of the interelectronic distance is separated by using error functions. According to Reference 106, we enforced the LC condition, that is, full exact exchange in the long-range limit, and chose the PBE functional for the relevant calculations. The value of the range-separation parameter γ was then determined non-empirically, but system-specific, such that the negative energy of the highest occupied molecular orbital (HOMO) is optimally close to the vertical ionization potential (IP). ¹⁰⁷ See Reference 106 for details and implications of this tuning (OT-RSH) in the context of optical rotation, and Reference 108 regarding molecular properties more generally. Minor differences in the γ parameters between different conformers of the same molecule were accounted for by Boltzmann averaging at room temperature, as detailed previously. The final VROA calculations employed one unique γ parameter per molecule, indicated as γ^* . All γ parameters are listed in **Section S2** of the Supporting Information.

An unbiased assessment of the similarity between calculated and experimental spectra is possible thanks to a variety of indicators that have been introduced. A detailed overview is presented in Reference 15. Our study employs SimROA indices as the most obvious choice to assess the similarity between experimental and calculated VROA spectra. Other indices

were shown to yield similar results,¹⁰⁹ and the conclusions based on the SimROA spectra can be easily extended to other indicators as well (see for example **Section S4** of the Supporting Information). Spectral vibrational frequency scaling factors, SimRaman and SimROA indices were calculated using the CDSpecTech program.¹⁰⁹ For brevity, only SimROA indices are reported in the article. SimRaman indices complementing the SimROA values are reported in **Section S4** of the Supporting Information. In the theory-experiment comparisons, only the scaling factors corresponding to the highest similarity with the experimental spectra are reported. SimROA indices were also determined from comparing different calculated spectra. In these cases, the frequency scaling factors are unity because in the computational setup chosen for this study the different VROA intensity calculations all share the same underlying B3LYP-D3(BJ)/def2-TZVP vibrational modes and frequencies. Spectra were visualized using CDSpecTech, PyVib2,¹¹⁰ and an in-house modified version of Exatomic.¹¹¹ Lorentzian broadening of the VROA transitions corresponding to a FWHM of 10 cm⁻¹ was applied. Experimental and theoretical spectra were obtained for a back-scattering arrangement, with the exception of molecules **18** and **19**, obtained in a right-angle scattering geometry.

In the original publications, the experimental spectra are reported in relative (arbitrary), not absolute, units for the cross sections or scattering intensities. For this reason, the figures in the main text and in the Supporting Information reporting experimental and calculated spectra show normalized intensities. Experimental spectra were digitized using the Web-PlotDigitizer program, version 4.4. The digitized xy data are provided in the Supporting Information.

3 The VROA36 Molecule Set

Figure 1 displays chemical drawings for the molecules included in VROA36. Their names, the experimental conditions used to record the VROA spectra, and relevant literature references, are collected in **Table 1**. The compounds represent typical samples analyzed with the help of VROA spectroscopy, focusing mostly on organic molecules but also including organometallic complexes. Experimental spectra for seven of the systems used an incident light wavelength of 488.0 nm, spectra for eight systems used an incident wavelength of 514.5 nm, and the remainder was recorded with the same incident wavelength of 532.0 nm that is used in commercial instruments.

Many of the molecules (1, 2, 3, 4, 5, 6, 7, 13, 14, 15, 16, 17, 20, and 24) have only one conformer, owing to their small size or rigidity. Also, only one conformer for 33, 34 and 35 was considered following references 95 and 113. In the original investigation of deuterated neopentane (29), 114,115 the authors took into account nine rotamers for this molecule,

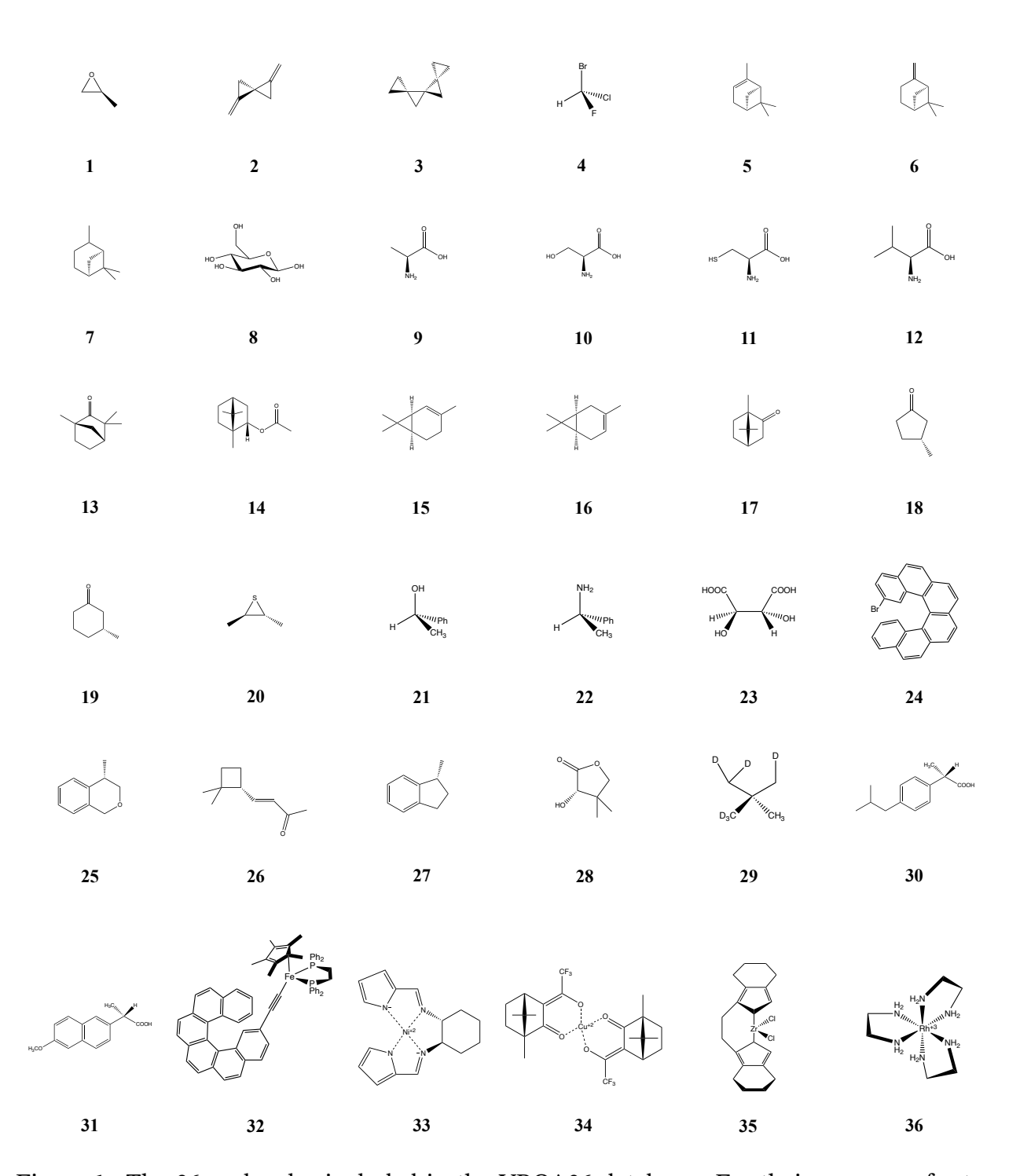


Figure 1: The 36 molecules included in the VROA36 database. For their names, refer to **Table 1**.

all based on the staggered geometry shown in **Figure 1**. The same approach is adopted here, and the reader is referred to **Section S10** of the Supporting Information for additional details. It is worth noting that this partially deuterated neopentane is chiral, while non-deuterated neopentane is not. Two conformers (boat and chair) were considered for **18**, **19**, **25**, **27**, and

28.

More than one conformer was considered for the more flexible molecules in the database. More specifically, three structures were included for glucose (8), two for L-alanine (9), six for L-serine and L-cysteine (10 and 11), eight for L-valine (12), five for phenylethanol (21), four for phenylethanamine (22), three for tartaric acid (23), seven for junionone (26), eight for ibuprofen (30), seven for naproxen (31), two for the iron helicene complex 32, and four for the rhodium complex 36. In total, the database includes 93 equilibrium geometries. XYZ structures are provided in the Supporting Information.

Table 1: Reference numbers, names, experimental conditions, and literature references for the experimental spectra of the VROA36 set. The numbers from the first column are used in **Figure 1** and in the text. Experimental spectra were recorded in a back-scattering setup, unless noted otherwise.

Numb	er Name	Experimental setup	Ref.
1	(S)-2-methyloxirane	Neat liquid; 532.0 nm	116,117
2	(S)-1,4-	Neat liquid; 532.0 nm	118
	dimethylenespiropentane		
3	(S)-trispirononane	Neat liquid; 532.0 nm	119
4	(R)-bromochlorofluoromethane	Neat liquid; 514.5 nm	120
5	$(-)$ - $(1S,5S)$ - α -pinene	Neat liquid; 488.0 nm	121
6	$(-)$ - $(1S,5S)$ - β -pinene	Neat liquid; 488.0 nm	122
7	(+)-trans-pinane	Neat liquid; 488.0 nm	121,122
8	d-glucose	Solution (water), 4.5 M;	123
		514.5 nm	
9	L-alanine	Solution (water), almost	124–126
		saturated; 488.0 nm	
10	L-serine	Solution (water), 1.78 M;	125
		514.5 nm	
11	L-cysteine	Solution (water), 1.31 M;	125
		514.5 nm	
12	L-valine	Solution (water), 0.38 M;	125
		514.5 nm	
13	(+)-fenchone	Neat liquid; 532.0 nm	127,128

14	Bornyl acetate	Neat liquid; 532.0 nm	
15	2-carene	Neat liquid; 532.0 nm	127,128
16	3-carene	3-carene Neat liquid; 532.0 nm	
17	Camphor	Solution (CCl ₄), 181 mg/ml;	130
		532.0 nm	
18	(R)-3-methylcyclopentanone	Neat liquid;	131
		488.0 nm; R-AS ^a	
19	(R)-3-methylcyclohexanone	Neat liquid;	132
		488.0 nm; R-AS ^a	
20	(2R,3R)-2,3-dimethylthiirane	Neat liquid; 488.0 nm	133
21	(R)-1-phenylethan-1-ol	Neat liquid; 532.0 nm	134
22	(R)-1-phenylethan-1-amine	Neat liquid; 532.0 nm	134
23	(2R,3R)-tartaric acid	Solution (water), 3.0 M;	135
		514.5 nm	
24	P-2-bromohexahelicene ^b	Solution (chloroform), 0.030 M;	136
		532.0 nm	
25	(4S)-methylisochromane	Neat liquid; 532.0 nm	137
26	(R)-junionone	Neat liquid; 532.0 nm	138
27	(R)-1-methylindane	532.0 nm ^{c,d}	139
28	(S)-pantolactone	Solution (water), 873 mM;	140
		532.0 nm	
29	(R) - $[^2H_1, ^2H_2, ^2H_3]$ -neopentane	Neat liquid; 532.0 nm	114,115
30	(S)-ibuprofen	Solution (CCl ₄), 0.21 M;	141
		514.5 nm	
31	(S)-naproxen ^b	Solution (water); 514.5 nm	141,142
32	Iron ethynylcarbo[6]helicene	Solution (CH ₂ Cl ₂), 0.003 M;	90
	$derivative^b$	532.0 nm	
33	(R,R)-(ppma) ₂ -cyclohexane	Solution (chloroform), 532.0	95
	$nickel(II)^{b,e}$	nm	
34	(R) -Cu $(tfc)_2^{b,f}$	Solution (chloroform), 0.18 M;	95, 143
		532.0 nm	
35	$(S,S)-(en-thind)_2-ZrCl_2^g$	Solution (chloroform), 176 mM;	113
		532.0 nm	
36	Δ -tris(en)rhodium(III) ^h	Solution (water), 0.625 M;	144
		532.0 nm	

 a Right-angle scattering; b Near-resonance conditions; c No other experimental conditions specified in reference 139; d The sign of the spectrum was changed to conform to modern conventions, see **Section 4.3**; e ppma = (pyrrol-2-ylmethyleneamine); f tfc = (3-trifluoroacetyl-camphorato) g en-thind = (ethylenebis(4,5,6,7-tetrahydro-1-indenyl)); h en = ethylenediamine

4 Results and Discussion

4.1 Comparison between calculated and experimental spectra.

To facilitate the comparison between experimental and calculated vibrational spectra, it is common to scale calculated vibrational frequencies by a factor that is both functional- and basis set-dependent. This is also the case for applications to VROA. 15, 109, 130 Scaling factors were determined in the present study based on maximizing the similarity between computed and experimental spectra. For brevity, Tables 2 and 3 list the average scaling factors calculated considering 32 of the 36 molecules in the database, while the full results are reported in Section S3 of the Supporting Information. The scaling factors excluded from the averaging belong to 32, 33, 34 and 36. The scaling factors for 32 could only be determined for the M11 functional (reported in the Supporting Information). For both B3LYP-D3(BJ) and ωB97X-D this molecule is under resonance, and the G16 program yielded unphysically large Raman intensities. The spectra for 33 and 34 include additional effects—other than the chiral Raman scattering—that could contribute to the ROA intensities recorded experimentally but that are not included in the computational setup. 95 The computed spectra are therefore not expected to reproduce the experimental analogues fully, and the resulting scaling factors were left out. The optimal scaling factor for 36 seemed rather large (see Table S11 in the Supporting Information), and we decided to limit it to 1.10. To keep the analysis unbiased, this scaling factor was also excluded. In summary, all scaling factors lie in the range 1.00 ± 0.10 .

Scaling factors determine the relative position of calculated and experimental peaks. The ideal scaling factor would be unity, resulting in a perfect match between calculated and experimental spectra. In most cases, the numbers shown in **Table 2** are close to 0.99 for all approximations. The minimum value is around 0.92, while the maximum is usually around 1.04 and up to 1.10 for some cases. The uniformity of the scaling factors is due to the usage of a good level of theory for geometry optimizations and frequency calculations. There is no substantial effect of either the basis set or the functional employed in the calculation of the VROA intensities. This behavior is expected, since the same vibrational normal modes are used with

Table 2: Scaling factors (average, minimum and maximum) obtained through comparison between experimental and calculated spectra for eight functional/basis set combinations.

Functional Basis set	B3LYP-D3(BJ) def2-SVPD	M11 def2-SVPD	ωB97X-D def2-SVPD	B3LYP-D3(BJ) def2-TZVPD ^a
Average ^b	0.981	0.981	0.983	0.979
Max value b	1.038	1.038	1.096	1.030
Min value	0.916	0.916	0.916	0.916
Functional	B3LYP-D3(BJ)	M11	ωB97X-D	γ*-LC-PBE
Basis set	aug-cc-pVDZ	aug-cc-pVDZ	aug-cc-pVDZ	aug-cc-pVDZ
Average ^b	0.981	0.981	0.982	0.981
Max value b	1.038	1.038	1.035	1.038
Min value	0.917	0.916	0.916	0.916

^aOnly 15 molecules considered; ^bSome scaling factors excluded, see text.

all functional/basis set combinations. It is reassuring to see that the numerical values in **Table 2** agree well with those reported in the past for IR data, 75,77,78 and for other molecules not included in VROA36. 145-147 Given its favorable performance, the B3LYP-D3(BJ)/def2-TZVP level of theory is recommended for geometry optimizations and frequency calculations, as already suggested in Reference 77.

The SimROA indices measure how well the calculated and experimental signs, the relative VROA intensities and the vibrational transition frequencies match. In this case as well, the closer the value is to unity, the better is the quality of the calculated intensities. The (averaged) numerical values for all functionals and basis sets are reported in **Table 3**, with additional detailed data available in **Sections S3** and **S5** of the Supporting Information. In some cases, the numerical values are quite low, especially for molecules whose spectra were recorded in aqueous solution. The lack of treatment of solvation effects in the calculations is likely one of the causes of this behavior (see **Section 4.4** below for additional details). Other possible causes besides solvent effects include the lack of vibronic coupling of the transitions, which can have a noticeable influence on the shape and intensity of the computed peaks (see deuterated naproxen and quinidine in Reference 103 as an example). For molecules in aqueous solution, another source of discrepancy between calculated and experimental spectra might be due to the pH-dependence of their structure, as it is the case for the amino acids (9–12) and naproxen (31).

Even for the cases with low SimROA indices, the different functional/basis set combinations perform quite similarly. The def2-SVPD and aug-cc-pVDZ basis sets yield SimROA indices that are identical for practical purposes. The maximum value varies between 0.72 and 0.80 depending on the level of theory, and in all sets of calculations this maximum corre-

Table 3: SimROA indices (average, minimum and maximum) obtained from the comparison of experimental and calculated spectra using eight functional/basis set combinations for the molecules in VROA36.

Functional Basis set	B3LYP-D3(BJ) def2-SVPD	M11 def2-SVPD	ωB97X-D def2-SVPD	B3LYP-D3(BJ) def2-TZVPD ^a
Average ^b	0.370	0.379	0.363	0.426
$Max value^b$	0.721	0.800	0.781	0.716
Min value	0.053	0.027	0.104	0.181
Functional	B3LYP-D3(BJ)	M11	ωB97X-D	γ*-LC-PBE
Basis set	aug-cc-pVDZ	aug-cc-pVDZ	aug-cc-pVDZ	aug-cc-pVDZ
Average ^b	0.370	0.381	0.363	0.367
Max value b	0.720	0.799	0.779	0.759
Min value	0.047	0.027	0.098	0.036

^aOnly 15 molecules considered; ^bSome molecules excluded, see text.

sponds to 2-bromohexahelicene (**24**). This result is consistent with the original publication. ¹³⁶ The inclusion of the damping parameter for resonance VROA (RROA) calculations does not change the shape of the spectrum significantly, a feature reflected in the SimROA indices calculated for the spectra under resonance (see **Table 6** in **Section 4.5**). On the other hand, a few molecules such as L-valine (**12**) produce very small (< 0.1) SimROA indices, with the lowest values ranging from 0.03 (M11/def2-SVPD) to 0.08 for a few functional/basis set combinations. For such cases, it is practically impossible to assign the AC using computational methods only. ¹⁰⁹ Caution is advised when interpreting the spectra, and it is recommended to obtain additional information using different chiroptical techniques before proceeding with the assignment.

4.2 Comparisons among calculated spectra.

The first goal of this section is to understand how the def2-SVPD and aug-cc-pVDZ basis sets compare with each other when used with all the functionals considered in this work. The second is to investigate the performance of each functional and see how they compare with each other when the same basis set is used. These comparisons are possible and meaningful, because the VROA calculations in this study were set up such that they are based on the same vibrational frequencies and modes for a given molecule (B3LYP-D3(BJ)/def2-TZVP). Thus, differences in the computed spectra are due to the VROA intensities only, from the dynamic response tensors (electric dipole-electric dipole, electric-dipole-magnetic dipole, and electric-dipole-electric-quadrupole) and their normal mode derivatives calculated with a given functional and basis. This is reflected in the value of the scaling factors being equal to unity. The

Table 4: SimROA indices (average, minimum and maximum) from the comparison of def2-SVPD calculated spectra with the reference aug-cc-pVDZ data.

Functional Basis set	B3LYP-D3(BJ) def2-SVPD ^a	$\begin{array}{c} \mathbf{M11} \\ \mathbf{def2}\text{-SVPD}^a \end{array}$	ω B97X-D def2-SVPD a
Average	0.984	0.989	0.980
Max value	1.000	1.000	1.000
Min value	0.862	0.933	0.832

^aReference basis set for each functional: aug-cc-pVDZ

SimROA indices therefore quantify the differences between the calculated intensities. See the **Appendix** for further details.

The average SimROA indices listed in **Table 4** show that the differences between the normalized intensities obtained with def2-SVPD and aug-cc-pVDZ are—on average—minimal for the three functionals considered (γ^* -LC-PBE is excluded from this analysis since it was used with aug-cc-pVDZ only). For most spectra, there are no substantial differences between the two basis sets, as shown by the SimROA indices in **Section S5** of the Supporting Information. However, when deviations from unity are indeed present, as in the case of complex 35 shown in **Figure 2**, they are usually due to either a small mismatch in the calculated intensities for some vibrational transitions, or because of a sign change for one or more peaks. For example, the overlapped spectra in Figure 2 show a consistently good performance of both basis sets with either B3LYP-D3(BJ) or M11. For ω B97X-D, instead, the overlapped spectrum highlights a slightly different intensity pattern in the region between 100 and 450 cm⁻¹. The most obvious difference is for the peak around 200 cm⁻¹, whose intensity is greater with def2-SVPD than with aug-cc-pVDZ. Despite such minimal differences, both basis sets reproduce the spectral features of this and the other molecules correctly, as shown in Figures S1-S36 of the Supporting Information, and they can both be used interchangeably. The convergence behavior of def2-SVPD towards its triple- ζ analogue def2-TZVPD is similar to what was reported for the aug-cc-pVDZ and aug-cc-pVTZ basis sets.⁵¹ The numerical results are reported in Table S32 in the Supporting Information, while visual comparisons are shown in Section S7.

The comparison of the four functionals combined with the same basis set yields the Sim-ROA indices collected in **Table 5**. Only the def2-SVPD values and spectra from **Figure 2** will be discussed, but the same conclusions apply to the data computed with aug-cc-pVDZ as well. The SimROA indices are slightly smaller than those reported for the basis set comparison discussed above. Different functionals might yield different intensities for the same vibrational transition, and this functional effect is more noticeable than a basis set effect (when compar-

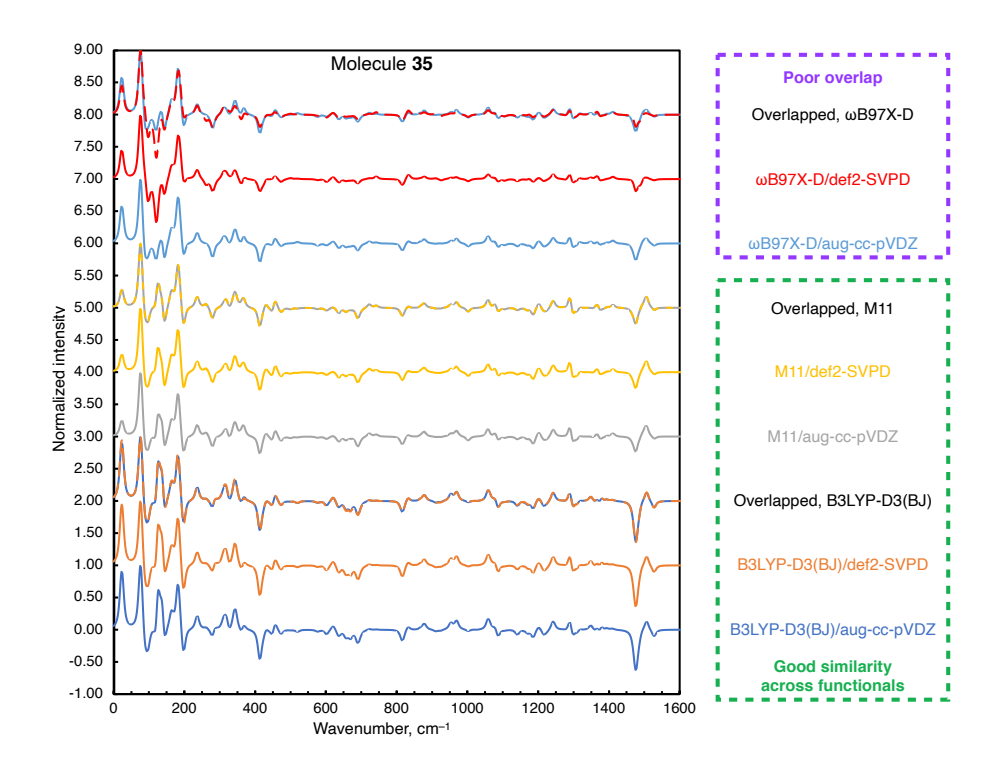


Figure 2: Spectra calculated with B3LYP-D3(BJ), M11 and ω B97X-D employing def2-SVPD or aug-cc-pVDZ for the zirconium complex (S,S)–(en–thind)₂–ZrCl₂, molecule **35**. For the overlapped spectra, solid curves are used to show the aug-cc-pVDZ results and dotted curves are used for def2-SVPD for each functional.

ing basis sets that are not altogether inadequate for the task at hand). This is clearly seen for the peak below 50 cm^{-1} in **Figure 2**. This peak is almost as intense as the one around 100 cm^{-1} when B3LYP-D3(BJ) is employed. The intensity calculated with M11 for the same transition is much smaller, while ω B97X-D yields a value in between. The intensities of the peaks around 400 and 1500 cm^{-1} are largest with B3LYP-D3(BJ) and smallest with ω B97X-D, while M11 is intermediate. The overall shape of the spectrum is preserved despite these differences.

The use of the OT-RSH functional (last column of **Table 5**) does not have a noticeable statistical effect on the spectral features. γ^* -LC-PBE appears closer to M11 than to ω B97X-D, which can be justified by looking at their range separation parameters (0.28 a_0^{-1} on average for γ^* -LC-PBE, 0.25 a_0^{-1} for M11, 0.20 a_0^{-1} for ω B97X-D). Overall, the four functionals show similar behavior, and the small differences highlighted by the SimROA indices do not hinder their successful application for VROA spectroscopy.

The analysis of the scaling factors and SimROA indices presented above reflects in part the trivial fact that the level of theory chosen for geometry optimization and frequency calculations must be appropriate such that the VROA spectra are not adversely affected. The B3LYP-

Table 5: Averaged SimROA indices calculated using the B3LYP-D3(BJ), M11, ω B97X-D, and γ^* -LC-PBE functionals with the basis sets aug-cc-pVDZ and def2-SVPD (in parentheses).

Functional	B3LYP-D3(BJ)	M11	ωB 97X-D	γ*-LC-PBE
B3LYP-D3(BJ)	$1.000 (1.000)^a$	$0.945 (0.943)^a$	$0.950 (0.951)^a$	0.977
M11	$0.945 (0.943)^a$	$1.000 (1.000)^a$	$0.942 (0.937)^a$	0.966
ω B97X-D	$0.950 (0.951)^a$	$0.942(0.937)^a$	$1.000 (1.000)^a$	0.960
γ^* -LC-PBE	0.977	0.966	0.960	1.000

^aThe values in parentheses are for the def2-SVPD basis set.

D3(BJ)/def2-TZVP combination is a satisfactory compromise in terms of accuracy and computational cost. For VROA intensities, the four functionals tested, namely B3LYP-D3(BJ), M11, ω B97X-D, and γ^* -LC-PBE are all good candidates. The def2-SVPD basis set is as reliable as aug-cc-pVDZ for the intensities, and it can be recommended for VROA calculations in conjunction with any of the hybrid functional approximations tested.

4.3 Visual comparison of the spectra.

In this section, a few representative experimental and calculated spectra are visually presented and analyzed. Spectra not shown here can be found in **Section S6** of the Supporting Information.

The molecules in the database can be divided in three groups based on the magnitude of the SimROA index obtained from comparing calculated and experimental spectra. Molecules in the first group have a SimROA index of at least 0.50. Compounds 1, 6, 7, 13, 14, 16, 17, 18, 20, 21, and 24 belong to this group. Molecules with SimROA indices between 0.25 and 0.50 belong to group 2, namely 2, 3, 4, 5, 8, 10, 15, 22, 28 and 29. The remainder (molecules 9, 11, 12, 19, 23, 25, 26, 27, 30, 31, 35, and 36) belong to the third group for which the SimROA index is below 0.25.

4.3.1 Molecules belonging to group 1. Example: S-methyloxirane.

S-methyloxirane has been extensively studied with theoretical methods, including TD-DFT and coupled cluster theory. ^{50,51,117,148} The experimental spectra were recorded in the gas and condensed phases, reported in **Figure 3** alongside the calculated spectra. All levels of theory yield a spectrum that is in excellent agreement with the experimental data. The three characteristic peaks of this molecule are between 700 and 900 cm⁻¹, all well reproduced by the calculations. The same is true for the signal around 1500 cm⁻¹. The calculated spectra seem to agree better with the spectrum recorded in the liquid phase, which is clearly a result of

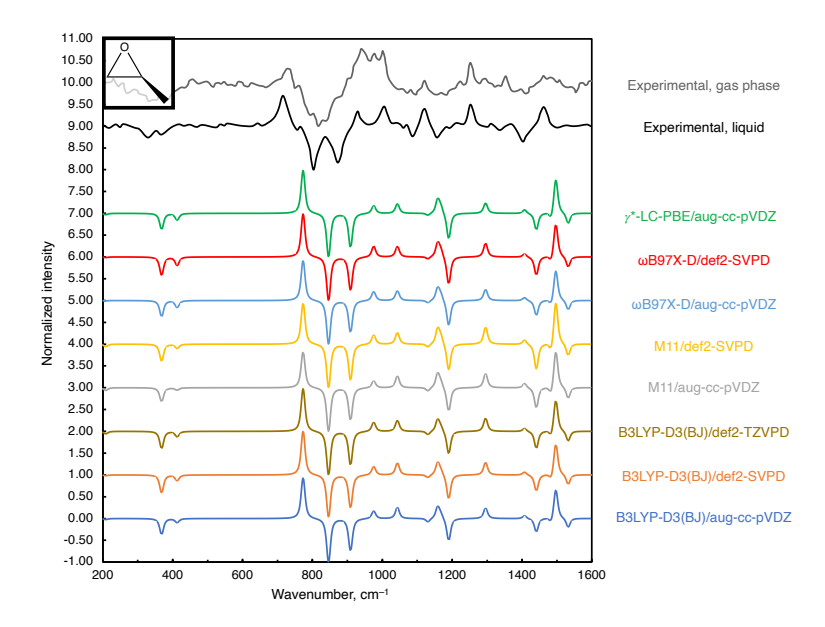


Figure 3: Calculated and experimental spectra for (S)-2-methyloxirane (1, shown in the top left corner). The experimental spectra were digitized from References 116 and 117. The incident wavelength is 532.0 nm. The calculated vibrational frequencies are unscaled.

error cancellation because no solvent effects or anharmonicity effects were accounted for in the calculations. For this species, there is little to no difference between the different functionals or basis sets. **Figure 3** also shows that even without frequency scaling, the calculated and experimental spectra agree well with each other. The calculations require a slight shift to lower frequency, with scaling factors around 0.97 as typical for DFT calculations.

4.3.2 Molecules belonging to group 2. Example: R-bromochlorofluoromethane

The VROA spectrum of R-bromochlorofluoromethane was experimentally characterized and its AC assigned in 1997¹²⁰ through one of the earliest applications of the combined experimental/computational VROA protocol. **Figure 4** shows that the calculated spectra agree failry well with the experiment, and they are consistent with the results published in Reference 120 where theoretical data were obtained with Møller-Plesset perturbation theory truncated at second order (MP2)¹⁴⁹ and a DZP basis. The main spectral features, i.e., the three peaks between 400 and 800 cm⁻¹, are all well reproduced by all functional and basis set combinations. All tested functionals, however, predict the wrong sign for the peaks around 250 and 1300 cm⁻¹, and only two functionals (ω B97X-D and γ *-LC-PBE) yield a peak around 1100 cm⁻¹ that matches the sign of the experimental signal but with a too low calculated intensity. The calculated spectra for this molecule are slightly shifted to lower frequency compared to the experiment.

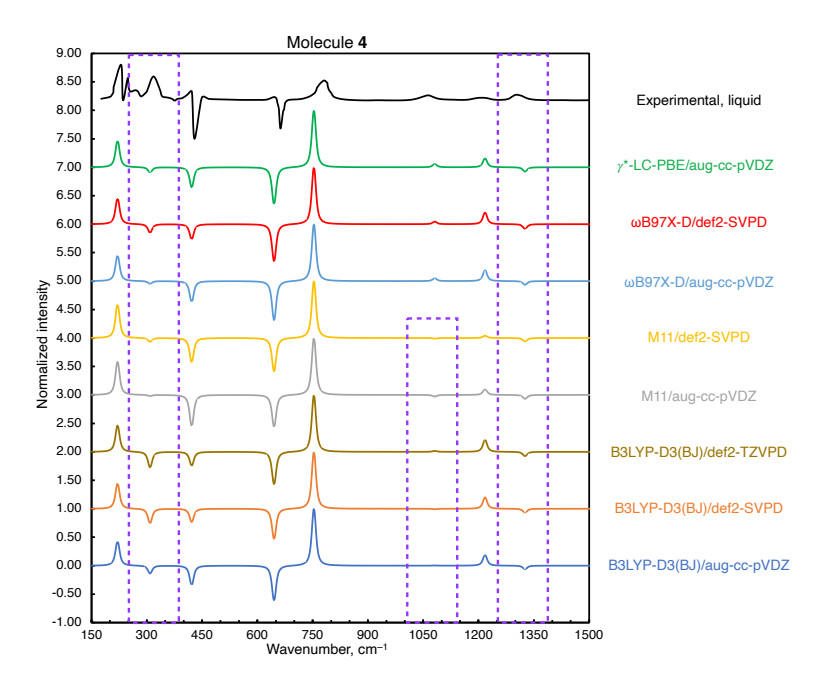


Figure 4: Calculated and experimental spectra for R-bromochlorofluoromethane (4). The experimental spectrum (black curve, neat liquid) were digitized from Reference 120. The incident wavelength is 514.5 nm. The calculated vibrational frequencies are unscaled.

4.3.3 Molecules belonging to group 3. Examples: R-methylindane and S-naproxen.

The AC of methylindane (27) was indirectly assigned for the first time in in 1966 using optical rotatory dispersion data from a series of closely-related molecules having R configuration. ¹⁵¹ Later, this assignment was revised using chemical correlations and ROA spectra, ¹³⁹ establishing the R enantiomer of this molecule as dextrorotatory, contrary to the previous findings. This application of VROA spectroscopy is one of the earliest reported.

Interestingly, the ROA intensities of the experimental spectrum in Reference 139 are reported as the differential scattering of circularly polarized light as Left minus Right, adopting the opposite convention of what is used nowadays. For consistency with the other experimental spectra, the black curve shown in **Figure 5** adopts the modern convention. Good agreement is found between the experimental and calculated spectra for the peaks observed in the low-frequency region between 200 and 500 cm⁻¹. They are similar in sign and intensity, although the peak around 600 cm⁻¹ is less intense than the experimental counterpart. The visual examination of the peaks above 800 cm⁻¹ is less informative, since there is no obvious relationship between the signals in the experimental and calculated spectra.

The spectra calculated for S-naproxen (31) are shown in **Figure 6**. All functionals and basis set give a consistent description of the spectrum, which appears with much more structure than the one recorded experimentally. All functionals yield spectra that are bisignate, which

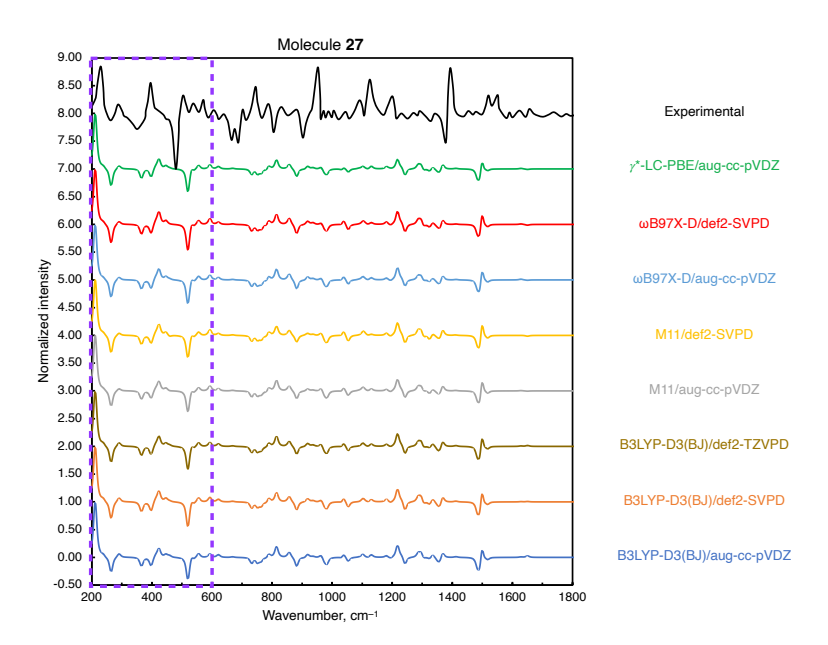


Figure 5: Experimental and conformationally averaged calculated spectra for R-methylindane (27). The experimental spectrum was digitized from Reference 139 and inverted to be consistent with modern VROA conventions (see text). The incident wavelength is 532.0 nm. The calculated vibrational frequencies are unscaled.

is not in agreement with the experimental reference. Baranska and co-workers reported that averaging spectra belonging to different conformers can result in the appearance in the final spectrum of peaks of both signs,¹⁵² an effect that is observed here as well. The most intense peak in the experimental spectrum is recorded around 1400 cm⁻¹, but no level of theory employed here is capable of replicating it. Further discussion of the naproxen spectrum can be found in **Section 4.5**.

4.4 A brief detour regarding the treatment of solvation effects.

The aim of this section is to show how the computed VROA spectra are impacted when solvation effects are taken into account in the calculations by means of one of the popular continuum solvation models. This section is not intended to be comprehensive, because solvation effects on molecular spectra can be rather complex and an in-depth assessment is far beyond the scope of the present study.

Proper treatment of solvation effects is a non-trivial task. The simplest way to include solvation effects in a spectrum is to use an implicit solvation model. More sophisticated techniques include the explicit modeling of solvent molecules as well as molecular dynamics simulations, with solvent molecules treated classically or quantum mechanically. The quality of the computed spectra is often improved with implicit solvation models, but such

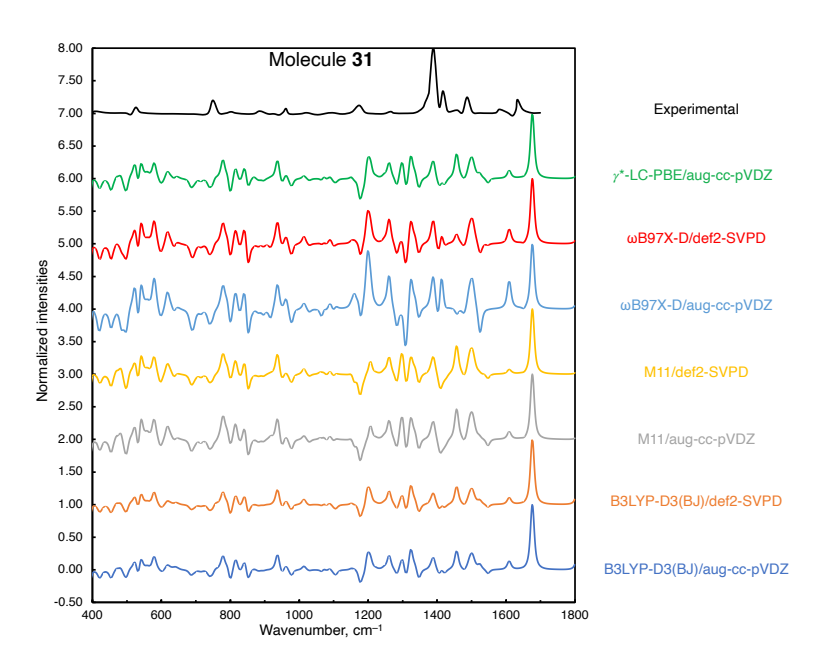


Figure 6: Conformationally averaged calculated and experimental spectra for S-naproxen (31). The experimental spectrum was digitized from references 141 and 142. The incident wavelength is 514.5 nm. The calculated vibrational frequencies are unscaled.

models may be inadequate when aqueous solutions are taken into consideration.^{154,155} For protic solvents such as water, the pH conditions used in the experimental setup can also affect the computed properties, as it is the case for amino acids, for example.¹⁵⁶ Therefore, the best computational strategy to include solvent effects depends both on the solvent and on the solute. Among the molecules in the database, d-glucose and camphor were selected as examples to discuss solvent effects as they are both polar molecules and thus susceptible to the polarization in the environment when it is treated with a continuum model.

The Boltzmann-averaged gas-phase spectrum of glucose is not in good agreement with the experiment, although some spectral features are already well reproduced, as shown in **Figure 7**, Panel **A**. Additional VROA calculations were performed using the C-PCM method on gas phase geometries (dotted lines, i.e. solvent effects are only considered for the polarizability tensors) and on the geometries optimized in presence of the solvent, affecting the normal modes as well. Adding solvent effects on top of the gas phase geometries results in smoothing out some of the shoulders in the peaks in the 1200–1300 cm⁻¹ region, while there is no noticeable difference compared to the spectra calculated from the re-optimized geometries. Better comparison with experiments can be achieved when a hybrid molecular mechanics/quantum mechanics approach is adopted¹⁵⁷ (red spectrum in Panel **A** of **Figure 7**, labeled as 'hybrid' in reference 157). Other studies^{158–160} have suggested that molecular dynamics simulations combined with the explicit introduction of water molecules are mandatory to obtain a sat-

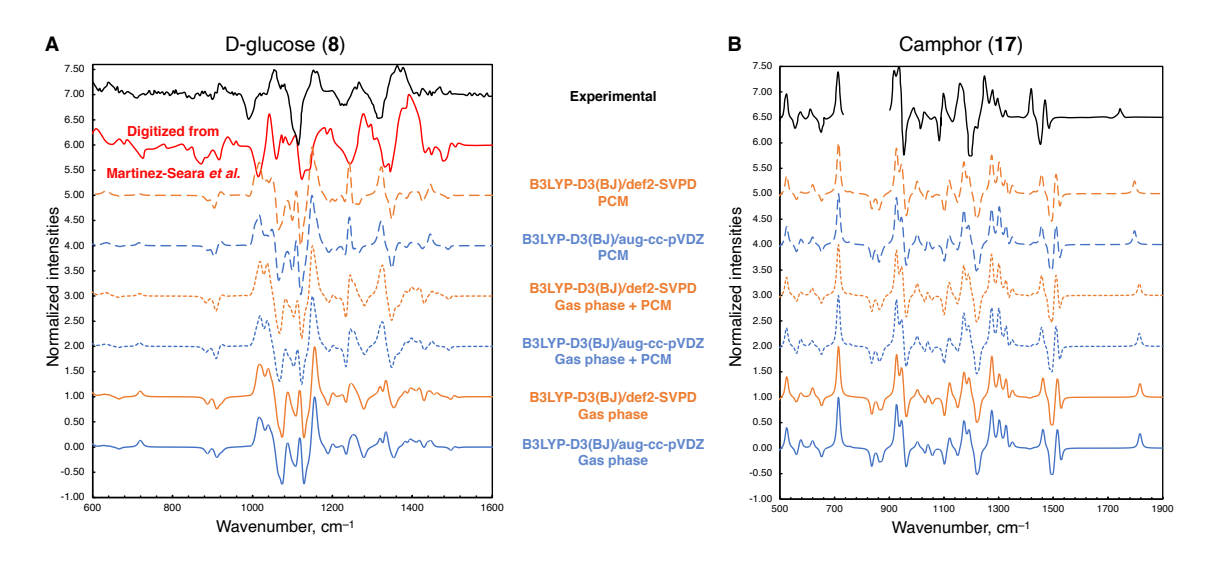


Figure 7: VROA spectra calculated for d-glucose (**8**, panel **A**) and camphor (**17**, panel **B**) with B3LYP-D3(BJ) and the aug-cc-pVDZ and def2-SVPD basis sets in different conditions. The spectrum reported in red was digitized from reference 157. The incident wavelength is 514.5 nm for d-glucose and 532.0 nm for camphor. Calculated vibrational frequencies are unscaled.

is factory agreement with the experimental data, although such approaches are also not free from short comings. 155,161

For camphor, instead, the Boltzmann-averaged gas-phase spectrum is in excellent agreement with the experimental reference, a result that may benefit from some favorable error cancellation. Inclusion of solvent effects has only a small effect on the computed intensities (**Figure 7**, Panel **B**). The intensity of one of the peaks around 1300 cm⁻¹ is increased in the presence of the continuum solvent model, while the peak around 1800 cm⁻¹ is shifted towards lower wavenumbers when compared with the gas phase spectra. For both molecules, the basis set does not have any effect on the computed intensities, and the spectral shapes are comparable in all cases.

For the two examples in this section, the changes due to the C-PCM do not drastically impact the similarity between experimental and calculated spectra. For d-glucose, an implicit solvation model is not suffcient to correctly reproduce the experimental spectrum, as it has been recognized in the literature on the subject. ^{157,162} In the case of camphor, the gas-phase calculation already produces a reasonable spectrum, and no harm is done when solvation effects are additionally included. In general, inclusion of an implicit solvation model is usually beneficial for research applications, ¹⁶² but the application of more sophisticated techniques may be required for more complicated cases.

Table 6: SimROA indices calculated using the B3LYP-D3(BJ) functional with the def2-SV(P), def2-SVPD, and aug-cc-pVDZ basis sets for the molecules studied under resonance conditions.

Molecule	def2-SV(P), RROA	def2-SVPD, RROA	aug-cc-pVDZ, RROA
24	0.718	$0.726 (0.721)^a$	$0.724 (0.720)^a$
31	0.266	$0.213 (0.217)^a$	$0.224 (0.222)^a$
32, averaged	0.697^{b}	c	0.690^d
33 , chloroform ^e	0.170	0.103	0.107
33 , dichloromethane ^e	0.053	0.050	0.058

^aThe values in parentheses are for the off-resonance cases;

4.5 Resonance ROA

In this section, the effect of the inclusion of a damping parameter Γ in the response calculations on the shape of the calculated spectra is examined. The five molecules analyzed are 2-bromohexahelicene (24), the lowest-energy conformer of S-naproxen (31), and the transition metal complexes 32, 33 and 34. The SimROA indices calculated for the molecules under resonance are reported in **Table 6**, while the corresponding scaling factors are reported in **Table S38**. Additional spectra for these species are shown in **Section S8** of the Supporting Information.

There is a visible enhancement of the intensities of the major peaks for 2-bromohexahelicene, especially those around 1400 and 1550 cm⁻¹ (**Figure 8**, panel **A**). Previous work has shown that the inclusion of Franck-Condon and Herzberg-Teller effects does not change the overall shape of the spectrum, although there is a small shift in the calculated peak from around 1550 cm⁻¹ in our spectrum to around 1600 cm⁻¹ in Figures 12 and 13 in Reference 103. Previous reports from our group showed that the def2-SV(P) basis set⁶⁴ correctly describes the chiroptical properties of helicenes, ^{90, 163, 164} as mentioned already. The spectrum shown in **Figure 8** as well as the first row of **Table 6** confirm again the good performance of this basis set for these compounds.

In the case of S-naproxen, the damped spectra are almost monosignate, especially in the experimentally-relevant region (900–1900 cm⁻¹, see panel **B** in **Figure 8**). The spectra obtained without damping are clearly bisignate, mostly due to the peaks below 1400 cm⁻¹, that are attenuated in the resonance setup. These results are consistent with a previous report, where the same molecule was analyzed at two different incident wavelengths (514.5 nm—used here as well—and 356.0 nm). The most intense peak is around 1400 cm⁻¹ in the experimental spectrum, while it is around 1900 cm⁻¹ for the computed spectra. This mismatch in

^bDifferent geometries, see text; ^cSee def2-SV(P);

^dcc-pVDZ basis set; ^eSome peaks excluded, see text.

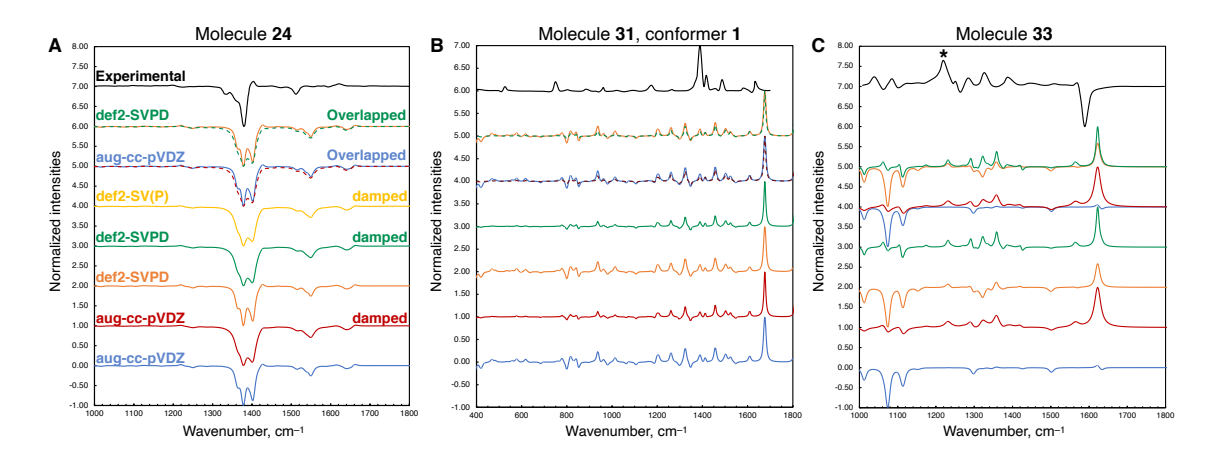


Figure 8: Damped and undamped spectra calculated with B3LYP-D3(BJ) and a few basis sets (aug-cc-pVDZ, def2-SV(P) and def2-SVPD) for 2-bromohexahelicene (panel **A**, left), the lowest-energy conformer of S-naproxen (panel **B**, middle) and the nickel complex (panel **C**, right). The overlap between undamped and damped spectra is also shown. The incident wavelength is 514.5 nm for naproxen and 532.0 nm for the other compounds.

the intensities is the likely cause of the low SimROA index in **Table 6**.

The nickel complex 33 shows a peculiar behavior: The signs of the spectra change from negative to positive with the inclusion of damping (Figure 8, panel C). The peak around 1250 cm⁻¹ was attributed to the solvent in reference 95, and thus excluded from the calculation of the SimROA indices in **Table 6**. Interestingly, all spectra appear almost monosignate. The spectra obtained without damping match the sign of the experimental reference, but they do not replicate the correct signals or the correct position of the peaks. The inclusion of damping results in a spectrum that is dominated by a peak around 1600 cm⁻¹. The position of this peak is close to the position of the experimental reference, but it is opposite in sign. The overall shape of the damped (and undamped) calculated spectra and the position of the signals closely resemble the computational results reported in Reference 95, which were obtained with B3LYP/aug-cc-pVTZ (see Figure S56 in the Supporting Information for a visual comparison of the near-resonance spectra). Despite a positive SimROA index due to a good match of the peaks in the 1300 cm⁻¹ region and especially when chloroform is used as solvent, it appears that the use of damping alone in the intensity calculations is not sufficient to reproduce the experimental spectrum of this molecule. Computational techniques that are capable of treating multiple light-matter interactions such as the eCP-Raman effect introduced in Reference 95 will be needed to obtain better agreement with the experimental spectra.

The Boltzmann averaged spectra for the iron complex **32** are reported in **Figure 9** (panel **A**), while those of the individual conformers are reported in **Section S8** of the Supporting

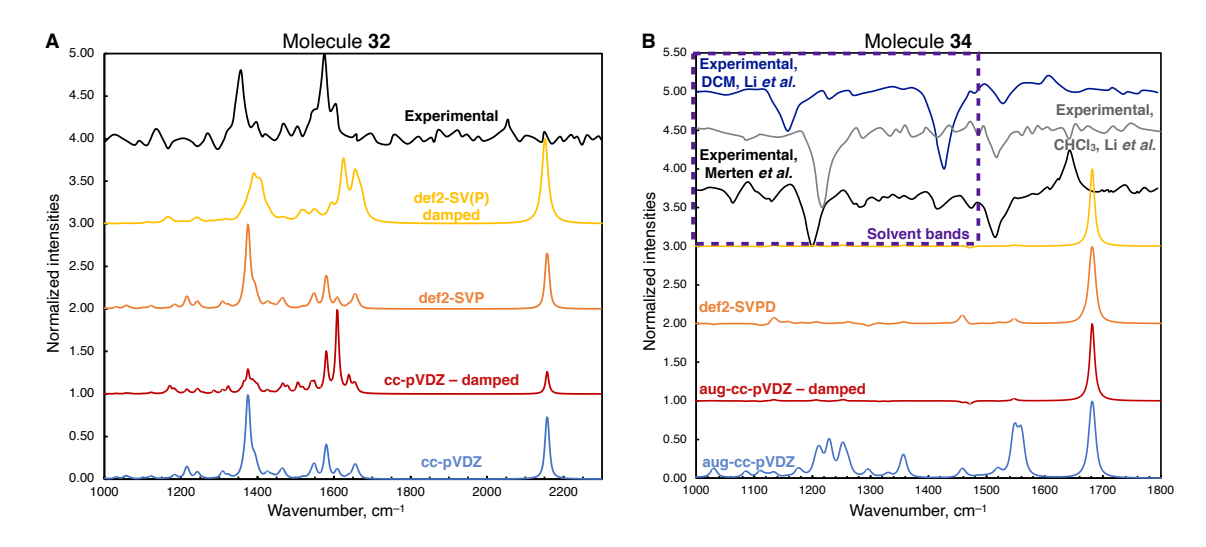


Figure 9: Damped and undamped averaged spectra calculated with B3LYP-D3(BJ) and the basis sets (aug-)cc-pVDZ and def2-SV(P) (or def2-SVPD) for the iron complex **32** (panel **A**) and the copper complex **34** (panel **B**). The incident wavelength is 532.0 nm.

Information. The undamped spectra obtained with B3LYP-D3(BJ) and cc-pVDZ or def2-SVP already show good agreement with the experimental data. The two characteristic groups of peaks are well-reproduced, although a slight shift towards higher frequencies is obtained in the calculations. A larger shift is observed for the transition around 2100 cm⁻¹, assigned to the stretching mode of the ethynyl unit that connects the helicene with the iron. Only the peak in the 1400 cm⁻¹ region matches the relative experimental intensity under off-resonance conditions. The relative intensities of the peaks' groups around 1600 cm⁻¹ and 2100 cm⁻¹ are better reproduced when damping is included, owing to the fact that the spectrum was recorded under conditions close to resonance. The effect of the damping is notable especially around 1600 cm⁻¹, and this results in a high SimROA index. This is even though the intensity of the alkynyl peak is rather strongly overestimated in most of the calculations.

Three experimental spectra are shown at the top of panel **B** of **Figure 9** for the copper complex **34**. Two were recorded in chloroform, ^{95, 143} the other in dichloromethane (Reference 95). The common feature of these spectra is the negative peak—attributed to the solute—around 1550 cm⁻¹, whereas the region below 1500 cm⁻¹ is dominated by solvent bands (see box in **Figure 9**). Another peak attributed to the solute is around 1650 cm⁻¹, although it is not clearly visible in the DCM spectrum. This peak however shows opposite sign in the two dichloromethane spectra, and the reason for this behavior is not clear. As briefly mentioned in **Section 4.1**, chiral Raman scattering might not be the only contribution to the recorded ROA intensities for this molecule, which rationalizes the disagreement between the experimental and calculated spectra. All calculated spectra appear monosignate, showing the most

intense peak around $1700 \, \mathrm{cm^{-1}}$. The spectral profile calculated with aug-cc-pVDZ shows other peaks between $1200 \, \mathrm{and} \, 1300 \, \mathrm{cm^{-1}}$ and around $1550 \, \mathrm{cm^{-1}}$ whose intensity is attenuated when the damping is introduced. The def2-SVPD (undamped) spectrum is dominated by the peak around $1700 \, \mathrm{cm^{-1}}$, and it is almost indistinguishable from the damped spectrum obtained with the def2-SV(P) basis set, or from the undamped spectrum produced by γ^* -LC-PBE (see **Figure S34** in the Supporting Information for this and other undamped spectra). The M11 functional produces a more complex spectral pattern, while the ω B97X-D is the only functional that is bisignate in the region between 1550 and 1650 cm⁻¹, and it also produces another signal slightly below 1500 cm⁻¹ that is not present in the experimental reference. Therefore, complex **34** exhibits a remarkable functional dependence of the calculated VROA, confirming the findings of Reference 95.

Overall, the (limited) choice of basis set does not influence the calculation of the ROA intensities for the on-resonance cases, as already observed for the off-resonance molecules. The def2-SVPD basis set can therefore be recommended in place of aug-cc-pVDZ for the resonance setup as well.

5 Summary and Conclusions

The VROA36 database of vibrational Raman optical activity spectra was introduced. VROA36 includes 36 molecules, covering both on- and off-resonance conditions. The database is composed of geometries for 93 molecular conformers optimized with B3LYP-D3(BJ)/def2-TZVP. The same functional/basis combination also yielded the vibrational modes and frequencies needed for further evaluation of four functionals, viz. B3LYP-D3(BJ), M11, ω B97X-D and the optimally tuned LC-PBE approximation, and three basis sets for the calculation of VROA intensities. The performance of the functionals was analyzed using frequency scaling factors and spectral SimROA indices determined from the comparison of calculated and experimental spectra, and of calculated spectra among each other.

This work showed that the B3LYP-D3(BJ)/def2-TZVP is a reliable and cost-effective choice to obtain good quality vibrational frequencies as a starting point for the calculation of ROA intensities. The four functionals employed with the aug-cc-pVDZ and def2-SVPD basis sets mostly showed very good agreement with the experimental references. When near-resonance cases were analyzed, the inclusion of a complex damping in the response calculations was found to be important to obtain physically meaningful VROA scattering intensities. As pointed out in recent literature, a full comparison with experimental spectra that were recorded under resonance may require the consideration of additional effects.

SimROA indices determined from the comparison of calculated spectra among each other

showed that aug-cc-pVDZ and def2-SVPD yield spectra of similar quality when combined with one of the tested functionals both under off- and on-resonance conditions. We therefore recommend the def2-SVPD basis set and any of the tested functionals approximations for theoretical VROA studies. The use of an optimally tuned range-separated hybrid functional has certain advantages (and disadvantages), as noted elsewhere in the general context of molecular property calculations. Similar to a previous study for optical rotation, there is no apparent harm being done by calculating VROA spectra with OT-RSH.

Appendix: Brief overview of the theory underlying VROA computations.

The quantity that needs to be computed for VROA is the differential absorption of left- and right-circularly polarized light, $I^R - I^L$. In a back-scattering setup, the ROA intensity is calculated according to **equation A-1** below,

$$I^{R}(180^{\circ}) - I^{L}(180^{\circ}) = K_{p} \left[\frac{48 \left(\beta (G')_{p}^{2} + \beta (A)_{p}^{2} \right) / 3}{90 c} \right]$$
 (A-1)

Here, $\beta(G')_p^2$ is the anisotropic invariant of the product of the electric dipole-magnetic dipole polarizability transition tensor and the electric dipole-electric dipole polarizability transition tensor (G' is also called gyration tensor). $\beta(A)_p^2$ is the anisotropic invariant of the product of the electric dipole-electric quadrupole polarizability transition tensor and the electric dipole-electric dipole-electric dipole transition polarizability tensor, c is the speed of light, and K_p is a frequency-dependent factor given as

$$K_p = \frac{\pi^2}{\epsilon_0^2} (\tilde{\nu}_{in} - \tilde{\nu}_p)^4 \frac{h}{8\pi^2 c \tilde{\nu}_p} \frac{1}{\exp[-hc\tilde{\nu}_p/(k_B T)]}$$
(A-2)

 K_p depends on the wave numbers of the incident frequency \tilde{v}_{in} and of the p-th vibrational normal mode \tilde{v}_p . Other quantities used in **equation A-2** are Planck's constant h, the Boltzmann constant k_B , the absolute temperature T, and the electric constant ϵ_0 . The vibrational wave numbers \tilde{v}_p depend on both the method (functional) and basis set used for the geometry optimization and frequency calculation steps. Inclusion of solvent effects affects these quantities too, since it has a direct effect on the geometries and—as a consequence—on the normal modes.

The tensor invariants of equation A-1 are

$$\beta(G')_p^2 = \operatorname{Im}\left(i\frac{3\alpha_{\alpha\beta}^p G_{\alpha\beta}^{\prime p*} - \alpha_{\alpha\alpha}^p G_{\beta\beta}^{\prime p*}}{2}\right) \tag{A-3a}$$

$$\beta(A)_p^2 = \operatorname{Re}\left(\frac{1}{2}\omega\alpha_{\alpha\beta}^p \epsilon_{\alpha\gamma\delta} A_{\gamma\delta\beta}^{p*}\right) \tag{A-3b}$$

where ω is the frequency of the incident laser and $\varepsilon_{\alpha\gamma\delta}$ is the Levi-Civita tensor. The quantities $\alpha_{\alpha\alpha}^p$, $\alpha_{\alpha\beta}^p$ are elements of the electric dipole-electric dipole polarizability tensor, $G'^p_{\alpha\alpha}$, $G'^p_{\alpha\beta}$ are elements of the gyration tensor, and $A^{p*}_{\gamma\delta\beta}$ is an element of the electric dipole-electric quadrupole polarizability tensor. Each of these quantities is calculated from taking the derivatives along the p-th vibrational normal mode (hence the superscript p), usually employing the TD-DFT framework due to its favorable performance-to-cost ratio. The quantities in **equations A-3a** and **A-3b** depend on the level of theory (*i.e.* method or functional and basis set).

The calculations performed in this study follow the 'two-step' procedure described by Cheeseman and Frisch in reference 51. In the first step, geometry optimizations and vibrational frequency calculations are performed using a given level of theory (B3LYP-D3(BJ)/def2-TZVP in this study). The Raman and ROA invariants are computed in the second step using all the information on geometries and vibrational normal modes from the Gaussian checkpoint files, thus allowing the usage of the same geometries and frequencies with different functional and basis set combinations. When the same vibrational normal modes are used, the differences in the calculated intensities depend on the functional used in the calculation of the response functions only (**equations A-3a** and **A-3b**), as mentioned at the beginning of **Section 4.2**.

The interested reader is referred to references 99 and 100 for details about the calculations with the NWChem code, and to reference 165 for more details about the units employed in this **Appendix**.

Acknowledgments

We acknowledge the Center for Computational Research (CCR) at the University at Buffalo for providing computational resources. P. M. is grateful to Dr. Cody Covington for help with the CDSpecTech program, and to Dr. James Cheeseman and Prof. Petr Bouř for providing structures for the nickel and copper complexes 33 and 34. We acknowledge the National Science Foundation for financial support of this research via grant CHE-1855470.

Supporting Information Available

Numerical values and plots of all calculated spectra. SimROA and SimRaman values calculated with the CDSpecTech program for each functional/basis set combination. Gibbs free energies, OT-RSH γ parameters for each compound, Boltzmann weights used to obtain the γ^* parameter for the LC-PBE functional. Molecular images and structures for each molecule. Output files from G16 and NWChem containing the raw computational data of the present study can be found at this link: https://dataverse.harvard.edu/dataverse/vroa36db (Accessed March 2022).

References

- [1] Eyring, H.; Liu, H.-C.; Caldwell, D. Optical Rotatory Dispersion and Circular Dichroism. *Chem. Rev.* **1968**, *68*, 525–540.
- [2] Caldwell, D. J.; Eyring, H. *The theory of optical activity;* Wiley-Interscience: New York, 1971.
- [3] Schellman, J. A. Circular dichroism and optical rotation. *Chem. Rev.* **1975**, *75*, 323–331.
- [4] Riehl, J. P.; Richardson, F. S. Circularly polarized luminescence spectroscopy. *Chem. Rev.* **1986**, *86*, 1–16.
- [5] Richardson, F. S.; Riehl, J. P. Circularly polarized luminescence spectroscopy. *Chem. Rev.* **1977**, *77*, 773–792.
- [6] Keiderling, T. A. Structure of Condensed Phase Peptides: Insights from Vibrational Circular Dichroism and Raman Optical Activity Techniques. *Chem. Rev.* **2020**, *120*, 3381–3419.
- [7] Johnson, W. C. Secondary Structure of Proteins Through Circular Dichroism Spectroscopy. *Annu. Rev. Biophys. Biophys. Chem.* **1988**, *17*, 145–166.
- [8] Albano, G.; Pescitelli, G.; Di Bari, L. Chiroptical Properties in Thin Films of π -Conjugated Systems. *Chem. Rev.* **2020**, *120*, 10145–10243.
- [9] He, Y.; Bo, W.; Dukor, R. K.; Nafie, L. A. Determination of Absolute Configuration of Chiral Molecules Using Vibrational Optical Activity: A Review. *Appl. Spectrosc.* **2011**, *65*, 699–723.

- [10] Nafie, L. A. Vibrational Optical Activity: Principles and Applications; Wiley: Chichester, West Sussex, 2011.
- [11] Barron, L. D.; Buckingham, A. D. Rayleigh and Raman scattering from optically active molecules. *Molecular Physics* **1971**, *20*, 1111–1119.
- [12] Barron, L. D.; Bogaard, M. P.; Buckingham, A. D. Raman Scattering of Circularly Polarized Light by Optically Active Molecules. *J. Am. Chem. Soc.* **1973**, *95*, 603–605.
- [13] Hug, W.; Kint, S.; Bailey, G. F.; Scherer, J. R. Raman Circular Intensity Differential Spectroscopy. Spectra of (-)-.Alpha.-Pinene and (+)-.Alpha.-Phenylethylamine. *J. Am. Chem. Soc.* **1975**, *97*, 5589–5590.
- [14] Blanch, E. Vibrational Raman Optical Activity of Proteins, Nucleic Acids, and Viruses. *Methods* **2003**, *29*, 196–209.
- [15] Polavarapu, P. L.; Covington, C. L. Comparison of Experimental and Calculated Chiroptical Spectra for Chiral Molecular Structure Determination. *Chirality* **2014**, *26*, 539–552.
- [16] Autschbach, J. Computing chiroptical properties with first–principles theoretical methods: Background and illustrative examples. *Chirality* **2009**, *21*, E116–E152.
- [17] Srebro-Hooper, M.; Autschbach, J. Calculating natural optical activity of molecules from first principles. *Annu. Rev. Phys. Chem.* **2017**, *68*, 399–420.
- [18] Hug, W. Visualizing Raman and Raman Optical Activity Generation in Polyatomic Molecules. *Chem. Phys.* **2001**, *264*, 53–69.
- [19] Pulay, P. Analytical derivative techniques and the calculation of vibrational spectra. In *Modern electronic structure theory Part II*, Vol. 2; Yarkony, D. R., Ed.; World Scientific: Singapore, 1995 1191–1240.
- [20] Bose, P.; Barron, L.; Polavarapu, P. Ab Initio and Experimental Vibrational Raman Optical Activity in (+)-(R)-Methylthiirane. *Chem. Phys. Lett.* **1989**, *155*, 423–429.
- [21] Autschbach, J.; Nitsch-Velasquez, L.; Rudolph, M. Time-dependent density functional response theory for electronic chiroptical properties of chiral molecules. *Top. Curr. Chem.* **2011**, *298*, 1–98.
- [22] Kohn, W.; Sham, L. Self-Consistent Equations Including Exchange and Correlation Effects. *Phys. Rev. A* **1965**, *140*, 1133–1138.

- [23] Morgante, P.; Peverati, R. The Devil in the Details: A Tutorial Review on Some Undervalued Aspects of Density Functional Theory Calculations. *Int. J. Quantum Chem.* **2020**, e26332.
- [24] Perdew, J. P.; Schmidt, K. Jacob's ladder of density functional approximations for the exchange-correlation energy. *AIP Conf. Proc.* **2001**, *577*, 1–20.
- [25] Goerigk, L.; Hansen, A.; Bauer, C.; Ehrlich, S.; Najibi, A.; Grimme, S. A Look at the Density Functional Theory Zoo with the Advanced GMTKN55 Database for General Main Group Thermochemistry, Kinetics and Noncovalent Interactions. *Phys. Chem. Chem. Phys.* **2017**, *19*, 32184–32215.
- [26] Mardirossian, N.; Head-Gordon, M. Thirty Years of Density Functional Theory in Computational Chemistry: An Overview and Extensive Assessment of 200 Density Functionals. *Mol. Phys.* **2017**, *115*, 2315–2372.
- [27] Yu, H. S.; He, X.; Li, S. L.; Truhlar, D. G. MN15: A Kohn–Sham Global-Hybrid Exchange–Correlation Density Functional with Broad Accuracy for Multi-Reference and Single-Reference Systems and Noncovalent Interactions. *Chem. Sci.* **2016**, *7*, 5032–5051.
- [28] Silva-Junior, M. R.; Schreiber, M.; Sauer, S. P. A.; Thiel, W. Benchmarks for electronically excited states: Time-dependent density functional theory and density functional theory based multireference configuration interaction. *J. Chem. Phys.* **2008**, *129*, 104103.
- [29] Caricato, M.; Trucks, G. W.; Frisch, M. J.; Wiberg, K. B. Electronic Transition Energies: A Study of the Performance of a Large Range of Single Reference Density Functional and Wave Function Methods on Valence and Rydberg States Compared to Experiment. *J. Chem. Theory Comput.* **2010**, *6*, 370–383.
- [30] Adamo, C.; Jacquemin, D. The calculations of excited-state properties with Time-Dependent Density Functional Theory. *Chem. Soc. Rev.* **2013**, *42*, 845–856.
- [31] Jacquemin, D.; Moore II, B.; Planchat, A.; Adamo, C.; Autschbach, J. Performance of an Optimally-Tuned Range-Separated Hybrid Functional for 0-0 Electronic Excitation Energies. *J. Chem. Theory Comput.* **2014**, *10*, 1677–1685.
- [32] Loos, P.-F.; Scemama, A.; Blondel, A.; Garniron, Y.; Caffarel, M.; Jacquemin, D. A Mountaineering Strategy to Excited States: Highly Accurate Reference Energies and Benchmarks. *J. Chem. Theory Comput.* **2018**, *14*, 4360–4379.

- [33] Migliore, A. How To Extract Quantitative Information on Electronic Transitions from the Density Functional Theory "Black Box". *J. Chem. Theory Comput.* **2019**, *15*, 4915–4923.
- [34] Loos, P.-F.; Lipparini, F.; Boggio-Pasqua, M.; Scemama, A.; Jacquemin, D. A Mountaineering Strategy to Excited States: Highly Accurate Energies and Benchmarks for Medium Sized Molecules. *J. Chem. Theory Comput.* **2020**, *16*, 1711–1741.
- [35] Loos, P.-F.; Scemama, A.; Boggio-Pasqua, M.; Jacquemin, D. Mountaineering Strategy to Excited States: Highly Accurate Energies and Benchmarks for Exotic Molecules and Radicals. *J. Chem. Theory Comput.* **2020**, *16*, 3720–3736.
- [36] Sarkar, R.; Boggio-Pasqua, M.; Loos, P.-F.; Jacquemin, D. Benchmarking TD-DFT and Wave Function Methods for Oscillator Strengths and Excited-State Dipole Moments. *J. Chem. Theory Comput.* **2021**, *17*, 1117–1132.
- [37] Haghdani, S.; Hoff, B. H.; Koch, H.; Åstrand, P.-O. Optical Rotation Calculations for Fluorinated Alcohols, Amines, Amides, and Esters. *J. Phys. Chem. A* **2016**, *120*, 7973–7986.
- [38] Haghdani, S.; Gautun, O. R.; Koch, H.; Åstrand, P.-O. Optical Rotation Calculations for a Set of Pyrrole Compounds. *J. Phys. Chem. A* **2016**, *120*, 7351–7360.
- [39] Haghdani, S.; Åstrand, P.-O.; Koch, H. Optical Rotation from Coupled Cluster and Density Functional Theory: The Role of Basis Set Convergence. *J. Chem. Theory Comput.* **2016**, *12*, 535–548.
- [40] Haghdani, S.; Hoff, B. H.; Koch, H.; Åstrand, P.-O. Solvent Effects on Optical Rotation: On the Balance between Hydrogen Bonding and Shifts in Dihedral Angles. *J. Phys. Chem. A* **2017**, *121*, 4765–4777.
- [41] Srebro, M.; Govind, N.; de Jong, W. A.; Autschbach, J. Optical Rotation calculated with Time-Dependent Density Functional Theory: The OR45 benchmark. *J. Phys. Chem. A* **2011**, *115*, 10930–10949.
- [42] Adamo, C.; Barone, V. Toward reliable density functional methods without adjustable parameters: The PBE0 model. *J. Chem. Phys.* **1999**, *110*, 6158–6170.
- [43] Ernzerhof, M.; Scuseria, G. E. Assessment of the Perdew–Burke–Ernzerhof exchange-correlation functional. *J. Chem. Phys.* **1999**, *110*, 5029–5036.

- [44] Becke, A. D. A new mixing of Hartree-Fock and local density-functional theories. *J. Chem. Phys.* **1993**, *98*, 1372–1377.
- [45] Lee, C.; Yang, W.; Parr, R. G. Development of the Colle-Salvetti correlation-energy formula into a functional of the electron density. *Phys. Rev. B* **1988**, *37*, 785–789.
- [46] Becke, A. D. Density-functional exchange-energy approximation with correct asymptotic behavior. *Phys. Rev. A* **1988**, *38*, 3098–3100.
- [47] Becke, A. D. Density–functional thermochemistry. III. The role of exact exchange. *J. Chem. Phys.* **1993**, *98*, 5648–5652.
- [48] Yanai, T.; Tew, D. P.; Handy, N. C. A new hybrid exchange-correlation functional using the Coulomb-attenuating method (CAM-B3LYP). *Chem. Phys. Lett.* **2004**, *393*, 51–57.
- [49] Rohrdanz, M. A.; Herbert, J. M. Simultaneous benchmarking of ground- and excited-state properties with long-range-corrected density functional theory. *J. Chem. Phys.* **2008**, *129*, 034107–9.
- [50] Reiher, M.; Liegeois, V.; Ruud, K. Basis set and density functional dependence of vibrational Raman optical activity calculations. *J. Phys. Chem. A* **2005**, *109*, 7567–7574.
- [51] Cheeseman, J. R.; Frisch, M. J. Basis Set Dependence of Vibrational Raman and Raman Optical Activity Intensities. *J. Chem. Theory Comput.* **2011**, 7, 3323–3334.
- [52] Slater, J. C. A Simplification of the Hartree-Fock-Method. *Phys. Rev.* **1951**, *3*, 385–390.
- [53] Vosko, S. H.; Wilk, L.; Nusair, M. Accurate spin-dependent electron liquid correlation energies for local spin density calculations: a critical analysis. *Can. J. Phys.* **1980**, *58*, 1200–1211.
- [54] Zuber, G.; Hug, W. Rarefied Basis Sets for the Calculation of Optical Tensors. 1. The Importance of Gradients on Hydrogen Atoms for the Raman Scattering Tensor. J. Phys. Chem. A 2004, 108, 2108–2118.
- [55] Dunning, T. H. Gaussian basis sets for use in correlated molecular calculations. I. The atoms boron through neon and hydrogen. *J. Chem. Phys.* **1989**, *90*, 1007–1023.
- [56] Cheeseman, J. R.; Frisch, M. J.; Devlin, F. J.; Stephens, P. J. Hartree-Fock and density functional theory ab initio calculation of optical rotations using GIAOs: basis set dependence. *J. Phys. Chem. A* **2000**, *104*, 1039–1046.

- [57] Crawford, T. D.; Stephens, P. J. Comparison of time-dependent density-functional theory and coupled cluster theory for the calculation of the optical rotations of chiral molecules. *J. Phys. Chem. A* **2008**, *112*, 1339–1345.
- [58] Campos, C. T.; Jorge, F. E.; Silva, T. P.; Coppo, M. R. Basis set convergence on optical rotation DFT calculations. *Chem. Phys. Lett.* **2010**, *494*, 170–173.
- [59] Howard, J. C.; Sowndarya S. V., S.; Ansari, I. M.; Mach, T. J.; Baranowska-Łączkowska, A.; Crawford, T. D. Performance of Property-Optimized Basis Sets for Optical Rotation with Coupled Cluster Theory. *J. Phys. Chem. A* **2018**, *122*, 5962–5969.
- [60] Baranowska, A.; Sadlej, A. J. Polarized basis sets for accurate calculations of static and dynamic electric properties of molecules. *J. Comput. Chem.* **2010**, *31*, 552–560.
- [61] Baranowska-Łączkowska, A.; Łączkowski, K. Z. The ORP Basis Set Designed for Optical Rotation Calculations. *J. Comput. Chem.* **2013**, *34*, 2006–2013.
- [62] Baranowska-Łączkowska, A.; Łączkowski, K. Z.; Henriksen, C.; Fernández, B. New Basis Set for the Evaluation of Specific Rotation in Flexible Biological Molecules in Solution. *J. Phys. Chem. A* **2018**, *122*, 5477–5483.
- [63] Aharon, T.; Caricato, M. Compact Basis Sets for Optical Rotation Calculations. *J. Chem. Theory Comput.* **2020**, *16*, 4408–4415.
- [64] Weigend, F.; Ahlrichs, R. Balanced basis sets of split valence, triple zeta valence and quadruple zeta valence quality for H to Rn: Design and assessment of accuracy. *Phys. Chem. Chem. Phys.* **2005**, *7*, 3295–3305.
- [65] Witte, J.; Neaton, J. B.; Head-Gordon, M. Push It to the Limit: Characterizing the Convergence of Common Sequences of Basis Sets for Intermolecular Interactions as Described by Density Functional Theory. *J. Chem. Phys.* **2016**, *144*, 194306.
- [66] Dohm, S.; Hansen, A.; Steinmetz, M.; Grimme, S.; Checinski, M. P. Comprehensive Thermochemical Benchmark Set of Realistic Closed-Shell Metal Organic Reactions. *J. Chem. Theory Comput.* **2018**, *14*, 2596–2608.
- [67] Morgante, P.; Peverati, R. Statistically Representative Databases for Density Functional Theory Via Data Science. *Phys. Chem. Chem. Phys.* **2019**, *21*, 19092–19103.
- [68] Maurer, L. R.; Bursch, M.; Grimme, S.; Hansen, A. Assessing Density Functional Theory for Chemically Relevant Open-Shell Transition Metal Reactions. *J. Chem. Theory Comput.* **2021**, *17*, 6134–6151.

- [69] Frisch, M. J.; Trucks, G. W.; Schlegel, H. B.; Scuseria, G. E.; Robb, M. A.; Cheeseman, J. R.; Scalmani, G.; Barone, V.; Petersson, G. A.; Nakatsuji, H.; Li, X.; Caricato, M.; Marenich, A. V.; Bloino, J.; Janesko, B. G.; Gomperts, R.; Mennucci, B.; Hratchian, H. P.; Ortiz, J. V.; Izmaylov, A. F.; Sonnenberg, J. L.; Williams-Young, D.; Ding, F.; Lipparini, F.; Egidi, F.; Goings, J.; Peng, B.; Petrone, A.; Henderson, T.; Ranasinghe, D.; Zakrzewski, V. G.; Gao, J.; Rega, N.; Zheng, G.; Liang, W.; Hada, M.; Ehara, M.; Toyota, K.; Fukuda, R.; Hasegawa, J.; Ishida, M.; Nakajima, T.; Honda, Y.; Kitao, O.; Nakai, H.; Vreven, T.; Throssell, K.; Montgomery, J. A. Jr.; Peralta, J. E.; Ogliaro, F.; Bearpark, M. J.; Heyd, J. J.; Brothers, E. N.; Kudin, K. N.; Staroverov, V. N.; Keith, T. A.; Kobayashi, R.; Normand, J.; Raghavachari, K.; Rendell, A. P.; Burant, J. C.; Iyengar, S. S.; Tomasi, J.; Cossi, M.; Millam, J. M.; Klene, M.; Adamo, C.; Cammi, R.; Ochterski, J. W.; Martin, R. L.; Morokuma, K.; Farkas, O.; Foresman, J. B.; Fox, D. J. "Gaussian 16 Revision C.01", Gaussian, Inc., Wallingford CT, 2016. URL: www.gaussian.com.
- [70] Grimme, S.; Ehrlich, S.; Goerigk, L. Effect of the damping function in dispersion corrected density functional theory. *Journal of Computational Chemistry* **2011**, *32*, 1456–1465.
- [71] Peverati, R.; Truhlar, D. G. Quest for a Universal Density Functional: The Accuracy of Density Functionals across a Broad Spectrum of Databases in Chemistry and Physics. *Phil. Trans. R. Soc. A* **2014**, *372*, 20120476.
- [72] Witte, J.; Goldey, M.; Neaton, J. B.; Head-Gordon, M. Beyond Energies: Geometries of Nonbonded Molecular Complexes as Metrics for Assessing Electronic Structure Approaches. *J. Chem. Theory Comput.* **2015**, *11*, 1481–1492.
- [73] Sirianni, D. A.; Alenaizan, A.; Cheney, D. L.; Sherrill, C. D. Assessment of Density Functional Methods for Geometry Optimization of Bimolecular van Der Waals Complexes. *J. Chem. Theory Comput.* **2018**, *14*, 3004–3013.
- [74] Morgante, P.; Peverati, R. CLB18: A New Structural Database with Unusual Carbon–Carbon Long Bonds. *Chem. Phys. Lett.* **2021**, *765*, 138281.
- [75] Alecu, I. M.; Zheng, J.; Zhao, Y.; Truhlar, D. G. Computational Thermochemistry: Scale Factor Databases and Scale Factors for Vibrational Frequencies Obtained from Electronic Model Chemistries. *J. Chem. Theory Comput.* **2010**, *6*, 2872–2887.

- [76] Fornaro, T.; Biczysko, M.; Monti, S.; Barone, V. Dispersion Corrected DFT Approaches for Anharmonic Vibrational Frequency Calculations: Nucleobases and Their Dimers. *Phys. Chem. Chem. Phys.* **2014**, *16*, 10112–10128.
- [77] Kesharwani, M. K.; Brauer, B.; Martin, J. M. L. Frequency and Zero-Point Vibrational Energy Scale Factors for Double-Hybrid Density Functionals (and Other Selected Methods): Can Anharmonic Force Fields Be Avoided?. *J. Phys. Chem. A* **2015**, *119*, 1701–1714.
- [78] Hanson-Heine, M. W. D. Benchmarking DFT-D Dispersion Corrections for Anharmonic Vibrational Frequencies and Harmonic Scaling Factors. *J. Phys. Chem. A* **2019**, 123, 9800–9808.
- [79] Barone, V.; Cossi, M. Quantum Calculation of Molecular Energies and Energy Gradients in Solution by a Conductor Solvent Model. *J. Phys. Chem. A* **1998**, *102*, 1995–2001.
- [80] Cossi, M.; Rega, N.; Scalmani, G.; Barone, V. Energies, Structures, and Electronic Properties of Molecules in Solution with the C-PCM Solvation Model. *J. Comput. Chem.* **2003**, *24*, 669–681.
- [81] Grimme, S. Exploration of Chemical Compound, Conformer, and Reaction Space with Meta-Dynamics Simulations Based on Tight-Binding Quantum Chemical Calculations. *J. Chem. Theory Comput.* **2019**, *15*, 2847–2862.
- [82] Pracht, P.; Bohle, F.; Grimme, S. Automated Exploration of the Low-Energy Chemical Space with Fast Quantum Chemical Methods. *Phys. Chem. Chem. Phys.* **2020**, *22*, 7169–7192.
- [83] Peverati, R.; Truhlar, D. G. Improving the Accuracy of Hybrid Meta-GGA Density Functionals by Range Separation. *J. Phys. Chem. Lett.* **2011**, *2*, 2810–2817.
- [84] Chai, J.-D.; Head-Gordon, M. Long-Range Corrected Hybrid Density Functionals with Damped Atom–Atom Dispersion Corrections. *Phys. Chem. Chem. Phys.* **2008**, *10*, 6615.
- [85] Kendall, R. A.; Dunning, T. H.; Harrison, R. J. Electron affinities of the first-row atoms revisited. Systematic basis sets and wave functions.. *Journal of Chemical Physics* **1992**, *96*, 6796.
- [86] Balabanov, N. B.; Peterson, K. A. Systematically convergent basis sets for transition metals. I. All-electron correlation consistent basis sets for the 3d elements Sc–Zn. *J. Chem. Phys.* **2005**, *123*, 64107.

- [87] Balabanov, N. B.; Peterson, K. A. Basis Set Limit Electronic Excitation Energies, Ionization Potentials, and Electron Affinities for the 3d Transition Metal Atoms: Coupled Cluster and Multireference Methods. *J. Chem. Phys.* **2006**, *125*, 074110.
- [88] Perdew, J. P.; Burke, K.; Ernzerhof, M. Generalized Gradient Approximation Made Simple. *Phys. Rev. Lett.* **1996**, *77*, 3865–3868.
- [89] Iikura, H.; Tsuneda, T.; Yanai, T.; Hirao, K. A long-range correction scheme for generalized-gradient-approximation exchange functionals. *J. Chem. Phys.* **2001**, *115*, 3540–3544.
- [90] Shen, C.; Srebro-Hooper, M.; Weymuth, T.; Krausbeck, F.; Lopez Navarrete, J. T.; Ramirez, F. J.; Nieto-Ortega, B.; Casado, J.; Reiher, M.; Autschbach, J.; Crassous, J. Redox-active Chiroptical Switching in Mono- and Bis-Iron-Ethynyl-Carbo[6]Helicenes Studied by Electronic and Vibrational Circular Dichroism and Resonance Raman Optical Activity. *Chem. Eur. J.* 2018, 24, 15067–15079.
- [91] Shen, C.; Loas, G.; Srebro-Hooper, M.; Vanthuyne, N.; Toupet, L.; Cador, O.; Paul, F.; López Navarrete, J. T.; Ramírez, F. J.; Nieto-Ortega, B.; Casado, J.; Autschbach, J.; Vallet, M.; Crassous, J. Iron Alkynyl Helicenes: Redox-Triggered Chiroptical Tuning in the IR and Near-IR Spectral Regions and Suitable for Telecommunications Applications. *Angew. Chem. Int. Ed.* 2016, 55, 8062–8066.
- [92] London, F. Theorie quantique des courants interatomiques dans les combinaisons aromatique. *J. Phys. Radium* **1937**, *8*, 397–409.
- [93] Krykunov, M.; Autschbach, J. Calculation of optical rotation with time–periodic magnetic field–dependent basis functions in approximate time–dependent density functional theory. *J. Chem. Phys.* **2005**, *123*, 114103.
- [94] Frisch, M.; Head-Gordon, M.; Pople, J. Direct Analytic SCF Second Derivatives and Electric Field Properties. *Chem. Phys.* **1990**, *141*, 189–196.
- [95] Li, G.; Alshalalfeh, M.; Yang, Y.; Cheeseman, J. R.; Bouř, P.; Xu, Y. Can One Measure Resonance Raman Optical Activity?. *Angew. Chem. Int. Ed.* **2021**, in press.
- [96] Aprà, E.; Bylaska, E. J.; de Jong, W. A.; Govind, N.; Kowalski, K.; Straatsma, T. P.; Valiev, M.; van Dam, H. J. J.; Alexeev, Y.; Anchell, J.; Anisimov, V.; Aquino, F. W.; Atta-Fynn, R.; Autschbach, J.; Bauman, N. P.; Becca, J. C.; Bernholdt, D. E.; Bhaskaran-Nair, K.; Bogatko, S.; Borowski, P.; Boschen, J.; Brabec, J.; Bruner, A.; Cauët, E.;

- Chen, Y.; Chuev, G. N.; Cramer, C. J.; Daily, J.; Deegan, M. J. O.; Dunning, T. H.; Dupuis, M.; Dyall, K. G.; Fann, G. I.; Fischer, S. A.; Fonari, A.; Früchtl, H.; Gagliardi, L.; Garza, J.; Gawande, N.; Ghosh, S.; Glaesemann, K.; Götz, A. W.; Hammond, J.; Helms, V.; Hermes, E. D.; Hirao, K.; Hirata, S.; Jacquelin, M.; Jensen, L.; Johnson, B. G.; Jónsson, H.; Kendall, R. A.; Klemm, M.; Kobayashi, R.; Konkov, V.; Krishnamoorthy, S.; Krishnan, M.; Lin, Z.; Lins, R. D.; Littlefield, R. J.; Logsdail, A. J.; Lopata, K.; Ma, W.; Marenich, A. V.; Martin del Campo, J.; Mejia-Rodriguez, D.; Moore, J. E.; Mullin, J. M.; Nakajima, T.; Nascimento, D. R.; Nichols, J. A.; Nichols, P. J.; Nieplocha, J.; Otero-de-la-Roza, A.; Palmer, B.; Panyala, A.; Pirojsirikul, T.; Peng, B.; Peverati, R.; Pittner, J.; Pollack, L.; Richard, R. M.; Sadayappan, P.; Schatz, G. C.; Shelton, W. A.; Silverstein, D. W.; Smith, D. M. A.; Soares, T. A.; Song, D.; Swart, M.; Taylor, H. L.; Thomas, G. S.; Tipparaju, V.; Truhlar, D. G.; Tsemekhman, K.; Van Voorhis, T.; Vázquez-Mayagoitia, Á.; Verma, P.; Villa, O.; Vishnu, A.; Vogiatzis, K. D.; Wang, D.; Weare, J. H.; Williamson, M. J.; Windus, T. L.; Woliński, K.; Wong, A. T.; Wu, Q.; Yang, C.; Yu, Q.; Zacharias, M.; Zhang, Z.; Zhao, Y.; Harrison, R. J. NWChem: Past, Present, and Future. J. Chem. Phys. 2020, *152*, 184102.
- [97] Autschbach, J. Computation of Optical Rotation using Time–Dependent Density Functional Theory. *Comput. Lett.* **2007**, *3*, 131–150.
- [98] Autschbach, J. Time-dependent density functional theory for calculating origin-independent optical rotation and rotatory strength tensors. *ChemPhysChem* **2011**, *12*, 3224–3235.
- [99] Abella, L.; Ludowieg, H. D.; Autschbach, J. Theoretical Study of the Raman Optical Activity Spectra of $[M(en)_3]^{3+}$ with M = Co, Rh. *Chirality* **2020**, *32*, 741–752.
- [100] Krausbeck, F.; Autschbach, J.; Reiher, M. Calculated Resonance Vibrational Raman Optical Activity Spectra of Naproxen and Ibuprofen. *J. Phys. Chem. A* **2016**, *120*, 9740–9748.
- [101] Jensen, L.; Autschbach, J.; Schatz, G. C. Finite lifetime effects on the polarizability within time-dependent density functional theory. *J. Chem. Phys.* **2005**, *122*, 224115.
- [102] Jensen, L.; Autschbach, J.; Krykunov, M.; Schatz, G. C. Resonance Vibrational Raman Optical Activity: A time-dependent density functional theory approach. *J. Chem. Phys.* **2007**, *127*, 134101.

- [103] Baiardi, A.; Bloino, J.; Barone, V. Time-Dependent Formulation of Resonance Raman Optical Activity Spectroscopy. *J. Chem. Theory Comput.* **2018**, *14*, 6370–6390.
- [104] Caricato, M.; Balduf, T. Origin Invariant Full Optical Rotation Tensor in the Length Dipole Gauge without London Atomic Orbitals. *J. Chem. Phys.* **2021**, *155*, 024118.
- [105] Toulouse, J.; Colonna, F.; Savin, A. Long-range–short-range separation of the electronelectron interaction in Density-Functional Theory. *Phys. Rev. A* **2004**, *70*, 062505.
- [106] Srebro, M.; Autschbach, J. Tuned Range-Separated Time-Dependent Density Functional Theory applied to Optical Rotation. *J. Chem. Theory Comput.* **2012**, *8*, 245–256.
- [107] Baer, R.; Livshits, E.; Salzner, U. Tuned Range-Separated Hybrids in Density Functional Theory. *Ann. Rev. Phys. Chem.* **2010**, *61*, 85–109.
- [108] Autschbach, J.; Srebro, M. Delocalization error and 'functional tuning' in Kohn-Sham calculations of molecular properties. *Acc. Chem. Res.* **2014**, *47*, 2592–2602.
- [109] Covington, C. L.; Polavarapu, P. L. CDSpecTech: A single software suite for multiple chiroptical spectroscopic analyses. *Chirality* **2017**, *29*, 178–192.
- [110] Fedorovsky, M. "PyVib2, a Program for Analyzing Vibrational Motion and Vibrational Spectra", 2007.
- [111] Marchenko, A.; Duignan, T.; Philips, A.; Badger, T. G.; Ludowieg, H. D.; Moore, B. "Exatomic: A unified platform for computational chemists", https://github.com/exa-analytics/exatomic, DOI: 10.5281/zenodo.1256873. Accessed 11/21.
- [112] Rohatgi, A. "WebPlotDigitizer", 2016 http://arohatgi.info/WebPlotDigitizer, v3.10.
- [113] Johannessen, C.; Hecht, L.; Merten, C. Comparative Study of Measured and Computed Raman Optical Activity of a Chiral Transition Metal Complex. *ChemPhysChem* **2011**, *12*, 1419–1421.
- [114] Hug, W.; Haesler, J. Is the Vibrational Optical Activity of (R)-[2H1,2H2,2H3]-Neopentane Measurable?. *Int. J. Quantum Chem.* **2005**, *104*, 695–715.
- [115] Haesler, J.; Schindelholz, I.; Riguet, E.; Bochet, C. G.; Hug, W. Absolute configuration of chirally deuterated neopentane. *Nature* **2007**, *446*, 526–529.

- [116] Bose, P. K.; Polavarapu, P. L.; Barron, L. D.; Hecht, L. Ab Initio and Experimental Raman Optical Activity in (+)-(R)-Methyloxirane. *J. Phys. Chem.* **1990**, *94*, 1734–1740.
- [117] Šebestík, J.; Bouř, P. Raman Optical Activity of Methyloxirane Gas and Liquid. *J. Phys. Chem. Lett.* **2011**, *2*, 498–502.
- [118] Hug, W.; Haesler, J.; Kozhushkov, S. I.; de Meijere, A. 1,4-Dimethylenespiropentane: A Unique Model System for Studying Fermi Resonance in Raman Optical Activity. *ChemPhysChem* **2007**, *8*, 1161–1169.
- [119] Hug, W.; Zuber, G.; de Meijere, A.; Khlebnikov, A. F.; Hansen, H.-J. Raman Optical Activity of a Purely σ -Bonded Helical Chromophore: (-)-(M)- σ -[4]Helicene. *Helv. Chim. Acta* **2001**, *84*, 1–21.
- [120] Costante, J.; Hecht, L.; Polavarapu, P. L.; Collet, A.; Barron, L. D. Absolute Configuration of Bromochlorofluoromethane from Experimental and Ab Initio Theoretical Vibrational Raman Optical Activity. *Angew. Chem. Int. Ed.* **1997**, *36*, 885–887.
- [121] Che, D.; Nafie, L. A. Isolation of Raman Optical Activity Invariants. *Chem. Phys. Lett.* **1992**, *189*, 35–42.
- [122] Barron, L. D.; Hecht, L.; Gargaro, A. R.; Hug, W. Vibrational Raman Optical Activity in Forward Scattering: Trans-Pinane and β -Pinene. *J. Raman Spectrosc.* **1990**, *21*, 375–379.
- [123] Bell, A. F.; Barron, L. D.; Hecht, L. Vibrational Raman Optical Activity Study of D-Glucose. *Carbohydr. Res.* **1994**, *257*, 11–24.
- [124] Barron, L.; Gargaro, A.; Hecht, L.; Polavarapu, P. Experimental and Ab Initio Theoretical Vibrational Raman Optical Activity of Alanine. *Spectrochim. Acta A* **1991**, *47*, 1001–1016.
- [125] Gargaro, A. R.; Barron, L. D.; Hecht, L. Vibrational Raman Optical Activity of Simple Amino Acids. *J. Raman Spectrosc.* **1993**, *24*, 91–96.
- [126] Yu, G.-S.; Freedman, T. B.; Nafie, L. A.; Deng, Z.; Polavarapu, P. L. Experimental Measurement and Ab Initio Calculation of Raman Optical Activity of L-Alanine and Its Deuterated Isotopomers. *J. Phys. Chem.* **1995**, *99*, 835–843.

- [127] Polavarapu, P. L.; Covington, C. L.; Chruszcz-Lipska, K.; Zajac, G.; Baranska, M. Vibrational Raman Optical Activity of Bicyclic Terpenes: Comparison between Experimental and Calculated Vibrational Raman, Raman Optical Activity, and Dimensionless Circular Intensity Difference Spectra and Their Similarity Analysis: Vibrational Raman Optical Activity of Bicyclic Terpenes. *J. Raman Spectrosc.* **2017**, *48*, 305–313.
- [128] Polavarapu, P. L.; Covington, C. L.; Chruszcz-Lipska, K.; Zajac, G.; Baranska, M. Erratum: Vibrational Raman Optical Activity of Bicyclic Terpenes: Comparison between Experimental and Calculated Vibrational Raman, Raman Optical Activity, and Dimensionless Circular Intensity Difference Spectra and Their Similarity Analysis. *J. Raman Spectrosc.* **2017**, *48*, 777–777.
- [129] Chruszcz-Lipska, K.; Blanch, E. W. *In Situ* Analysis of Chiral Components of Pichtae Essential Oil by Means of ROA Spectroscopy: Experimental and Theoretical Raman and ROA Spectra of Bornyl Acetate: ROA Spectral Analysis of Bornyl Acetate in Pichtae Essential Oil. *J. Raman Spectrosc.* **2012**, *43*, 286–293.
- [130] Johnson, J. L.; Zajac, G.; Baranska, M.; Polavarapu, P. L. Vibrational Raman Optical Activity of Camphor: The Importance of Electric-dipole—Electric-quadrupole Polarizability Contribution. *J. Raman Spectrosc.* **2020**, *51*, 669–679.
- [131] Polavarapu, P. L.; Bose, P. K.; Hecht, L.; Barron, L. D. Vibrational Raman Optical Activity in (R)-(+)-3-Methylcyclopentanone: Experimental and Ab Initio Theoretical Studies. *J. Phys. Chem.* **1993**, *97*, 11211–11215.
- [132] Polavarapu, P. L.; Black, T. M.; Barron, L. D.; Hecht, L. Vibrational Raman Optical Activity in (R)-(+)-3-Methylcyclohexanone: Experimental and Ab Initio Theoretical Studies and the Origins of the Unusual Couplets. *J. Am. Chem. Soc.* **1993**, *115*, 7736–7742.
- [133] Polavarapu, P. L.; Pickard, S. T.; Smith, H. E.; Black, T. M.; Barron, L. D.; Hecht, L. Determination of Absolute Configurations from Vibrational Raman Optical Activity: Trans-2,3-Dimethylthiirane. *Talanta* **1993**, *40*, 545–549.
- [134] Kapitan, J.; Johannessen, C.; Bour, P.; Hecht, L.; Barron, L. Vibrational Raman Optical Activity of 1-Phenylethanol and 1-Phenylethylamine: Revisiting old friends. *Chirality* **2009**, *21*, E4–E12.

- [135] Barron, L.; Gargaro, A.; Hecht, L.; Polavarapu, P.; Sugeta, H. Experimental and Ab Initio Theoretical Vibrational Raman Optical Activity of Tartaric Acid. *Spectrochim. Acta A* **1992**, *48*, 1051–1066.
- [136] Johannessen, C.; Blanch, E. W.; Villani, C.; Abbate, S.; Longhi, G.; Agarwal, N. R.; Tommasini, M.; Lightner, D. A. Raman and ROA Spectra of (-)- and (+)-2-Br-Hexahelicene: Experimental and DFT Studies of a π -Conjugated Chiral System. *J. Phys. Chem. B* **2013**, *117*, 2221–2230.
- [137] Zuber, G.; Hug, W. Computational Interpretation of Vibrational Optical Activity: The ROA Spectra of (4S)-4-Methylisochromane and the (4S)-Isomers of Galaxolide®. *Helv. Chim. Acta* **2004**, *87*, 2208–2234.
- [138] Lovchik, M. A.; Fráter, G.; Goeke, A.; Hug, W. Total Synthesis of Junionone, a Natural Monoterpenoid from Juniperus Communis L., and Determination of the Absolute Configuration of the Naturally Occurring Enantiomer by ROA Spectroscopy. *C&B* **2008**, *5*, 126–139.
- [139] Hansen, H.-J.; Sliwka, H.-R.; Hug, W. The Absolute Configuration of 1-Methylindane. *Helv. Chim. Acta* **1979**, *62*, 1120–1128.
- [140] Ghidinelli, S.; Abbate, S.; Koshoubu, J.; Araki, Y.; Wada, T.; Longhi, G. Solvent Effects and Aggregation Phenomena Studied by Vibrational Optical Activity and Molecular Dynamics: The Case of Pantolactone. *J. Phys. Chem. B* **2020**, *124*, 4512–4526.
- [141] Vargek, M.; Freedman, T. B.; Lee, E.; Nafie, L. A. Experimental observation of resonance Raman optical activity. *Chem. Phys. Lett.* **1998**, *287*, 359 364.
- [142] Vargek, M.; Freedman, T. B.; Nafie, L. A. Resonance and Non-Resonance Raman Optical Activity in Pharmaceutical Analgesic Molecules. In *Spectroscopy of Biological Molecules: Modern Trends*; Carmona, P.; Navarro, R.; Hernanz, A., Eds.; Springer Netherlands: Dordrecht, 1997 459–460.
- [143] Merten, C.; Li, H.; Nafie, L. A. Simultaneous Resonance Raman Optical Activity Involving Two Electronic States. *J. Phys. Chem. A* **2012**, *116*, 7329–7336.
- [144] Humbert-Droz, M.; Oulevey, P.; Lawson Daku, L. M.; Luber, S.; Hagemann, H.; Bürgi, T. Where does the Raman optical activity of [Rh(en)₃]³⁺ come from? Insight from a combined experimental and theoretical approach. *Phys. Chem. Chem. Phys.* **2014**, *16*, 23260–23273.

- [145] Liegeois, V.; Champagne, B. Vibrational Raman optical activity of π -conjugated helical systems: Hexahelicene and heterohelicenes. *J. Comput. Chem.* **2009**, *30*, 1261–1278.
- [146] Liégeois, V.; Champagne, B. Theoretical Investigation of Raman Optical Activity Signatures of Tröger's Base. *J. Phys. Chem. A* **2011**, *115*, 13706–13713.
- [147] Daugey, N.; Brotin, T.; Vanthuyne, N.; Cavagnat, D.; Buffeteau, T. Raman Optical Activity of Enantiopure Cryptophanes. *J. Phys. Chem. B* **2014**, *118*, 5211–5217.
- [148] Crawford, T. D.; Ruud, K. Coupled-Cluster Calculations of Vibrational Raman Optical Activity Spectra. *ChemPhysChem* **2011**, *12*, 3442–3448.
- [149] Møller, C.; Plesset, M. S. Note on an approximation treatment for many-electron systems. *Phys. Rev.* **1934**, *46*, 618–622.
- [150] Dunning, T. H.; Hay, P. J. Gaussian Basis Sets for Molecular Calculations. In *Methods of Electronic Structure Theory*; Schaefer, H. F., Ed.; Springer US: Boston, MA, 1977 1–27.
- [151] Brewster, J. H.; Buta, J. G. Conformational Mobility and Optical Rotation Effects of Aromatic Nuclei¹. *J. Am. Chem. Soc.* **1966**, *88*, 2233–2240.
- [152] Zajac, G.; Kaczor, A.; Chruszcz-Lipska, K.; Dobrowolski, J. C.; Baranska, M. Bisignate Resonance Raman Optical Activity: A Pseudo Breakdown of the Single Electronic State Model of RROA?. *J. Raman Spectrosc.* **2014**, *45*, 859–862.
- [153] Ryu, H.; Park, J.; Kim, H. K.; Park, J. Y.; Kim, S.-T.; Baik, M.-H. Pitfalls in Computational Modeling of Chemical Reactions and How To Avoid Them. *Organometallics* **2018**, *37*, 3228–3239.
- [154] Pecul, M. Modeling of Solvation Effects on Chiroptical Spectra. In *Comprehensive Chiroptical Spectroscopy*; Berova, N.; Polavarapu, P. L.; Nakanishi, K.; Woody, R. W., Eds.; John Wiley & Sons, Inc.: Hoboken, NJ, USA, 2012 729–745.
- [155] Hopmann, K. H.; Ruud, K.; Pecul, M.; Kudelski, A.; Dračinský, M.; Bouř, P. Explicit versus Implicit Solvent Modeling of Raman Optical Activity Spectra. *J. Phys. Chem. B* **2011**, *115*, 4128–4137.
- [156] Kundrat, M. D.; Autschbach, J. Computational Modeling of the Optical Rotation of Amino Acids: Taking a New Look at an Old Rule for the pH Dependence of the Optical Rotation. *J. Am. Chem. Soc.* **2008**, *130*, 4404–4414.

- [157] Palivec, V.; Kopecký, V.; Jungwirth, P.; Bouř, P.; Kaminský, J.; Martinez-Seara, H. Simulation of Raman and Raman Optical Activity of Saccharides in Solution. *Phys. Chem. Chem. Phys.* **2020**, *22*, 1983–1993.
- [158] Cheeseman, J. R.; Shaik, M. S.; Popelier, P. L. A.; Blanch, E. W. Calculation of Raman Optical Activity Spectra of Methyl-β-D-Glucose Incorporating a Full Molecular Dynamics Simulation of Hydration Effects. *J. Am. Chem. Soc.* **2011**, *133*, 4991–4997.
- [159] Giovannini, T.; Del Frate, G.; Lafiosca, P.; Cappelli, C. Effective Computational Route towards Vibrational Optical Activity Spectra of Chiral Molecules in Aqueous Solution. *Phys. Chem. Chem. Phys.* **2018**, *20*, 9181–9197.
- [160] Polavarapu, P. L.; Santoro, E. Vibrational Optical Activity for Structural Characterization of Natural Products. *Nat. Prod. Rep.* **2020**, *37*, 1661–1699.
- [161] Tajkhorshid, E.; Jalkanen, K. J.; Suhai, S. Structure and Vibrational Spectra of the Zwitterion L-Alanine in the Presence of Explicit Water Molecules: A Density Functional Analysis. *J. Phys. Chem. B* **1998**, *102*, 5899–5913.
- [162] Krupová, M.; Kessler, J.; Bouř, P. Recent Trends in Chiroptical Spectroscopy: Theory and Applications of Vibrational Circular Dichroism and Raman Optical Activity. *ChemPlusChem* **2020**, *85*, 561–575.
- [163] Shen, C.; Srebro-Hooper, M.; Jean, M.; Vanthuyne, N.; Toupet, L.; Williams, J. A. G.; Torres, A. R.; Riives, A. J.; Muller, G.; Autschbach, J.; Crassous, J. Synthesis and chiroptical properties of hexa-, octa- and deca-azaborahelicenes: influence of the helicene's size and of the number of boron atoms. *Chem. Eur. J.* **2017**, *23*, 407–418.
- [164] Gauthier, E. S.; Abella, L.; Hellou, N.; Darquie, B.; Caytan, E.; Roisnel, T.; Vanthuyne, N.; Favereau, L.; Srebro-Hooper, M.; Williams, J. A. G.; Autschbach, J.; Crassous, J. Long-lived circularly-polarized phosphorescence in helicene-NHC-rhenium(I) complexes: The influence of helicene, halogen and stereochemistry on emission properties. *Angew. Chem. Int. Ed.* **2020**, *59*, 8394–8400.
- [165] Neugebauer, J.; Reiher, M.; Kind, C.; Hess, B. A. Quantum chemical calculation of vibrational spectra for large molecules Raman and IR spectra for Buckminsterfullerene. *J. Comput. Chem.* **2002**, *23*, 895–910.

Table of Contents Graphics

